

Article

New Structural Nanocomposite Based on PLGA and Al₂O₃ NPs as a Balance between Antibacterial Activity and Biocompatibility with Eukaryotic Cells

Alexander V. Simakin ^{1,*}, Ruslan M. Sarimov ¹, Veronika V. Smirnova ¹, Maxim E. Astashev ^{1,2}, Dmitriy A. Serov ^{1,2}, Denis V. Yanykin ^{1,2}, Denis N. Chausov ¹, Alexey V. Shkirin ¹, Oleg V. Uvarov ¹, Evgeny Rotanov ³, Andrey Shakhovskoy ³, Vadim I. Bruskov ⁴, Vladimir E. Ivanov ⁴, Alexey S. Dorokhov ⁵ and Andrey Y. Izmailov ⁵

¹ Prokhorov General Physics Institute of the Russian Academy of Sciences, 119991 Moscow, Russia

² Federal Research Center "Pushchino Scientific Center for Biological Research of the Russian Academy of Sciences", 142290 Pushchino, Russia

³ Research Department, K.G. Razumovsky Moscow State University of Technologies and Management (The First Cossack University), 73, Zemlyanoy Val St., 109004 Moscow, Russia

⁴ Institute of Theoretical and Experimental Biophysics of the Russian Academy of Sciences, 142290 Pushchino, Russia

⁵ Federal State Budgetary Scientific Institution "Federal Scientific Agroengineering Center VIM" (FSAC VIM), 109428 Moscow, Russia

* Correspondence: avsimakin@gmail.com



Citation: Simakin, A.V.; Sarimov, R.M.; Smirnova, V.V.; Astashev, M.E.; Serov, D.A.; Yanykin, D.V.; Chausov, D.N.; Shkirin, A.V.; Uvarov, O.V.; Rotanov, E.; et al. New Structural Nanocomposite Based on PLGA and Al₂O₃ NPs as a Balance between Antibacterial Activity and Biocompatibility with Eukaryotic Cells. *J. Compos. Sci.* **2022**, *6*, 298. <https://doi.org/10.3390/jcs6100298>

Academic Editors: Francesco Tornabene, Goshtasp Cheraghian and Tien-Thinh Le

Received: 8 July 2022

Accepted: 29 September 2022

Published: 9 October 2022

Publisher's Note: MDPI stays neutral with regard to jurisdictional claims in published maps and institutional affiliations.



Copyright: © 2022 by the authors. Licensee MDPI, Basel, Switzerland. This article is an open access article distributed under the terms and conditions of the Creative Commons Attribution (CC BY) license (<https://creativecommons.org/licenses/by/4.0/>).

Abstract: Development of eco-friendly and biodegradable package materials is an important goal of modern science and international industry. Poly(lactic)-co-glycolic acid (PLGA) is suitable for this purpose. However, biocompatible materials may be contaminated with bacteria. This problem may be solved by the addition of metal oxides nanoparticles (NPs) with antibacterial properties. Although metal oxides NPs often show cytotoxicity against plant and mammalian cells, a new nanocomposite based on PLGA and aluminum oxide (Al₂O₃) NPs has been developed. The PLGA/Al₂O₃ NP composite has pronounced antibacterial properties. The addition of Al₂O₃ NPs 0.01% inhibited growth of *E. coli* for >50%. The antimicrobial effect of Al₂O₃ NPs is implemented through the generation of reactive oxygen species and damage of bacterial proteins and DNA. The biocompatibility of the nanocomposite with plant and mammalian cells was studied. The PLGA/Al₂O₃ NP composite did not influence the growth and development of tomatoes and cucumbers. PLGA and its composite with Al₂O₃ NPs 0.001–0.1% did not influence viability and proliferation of mammalian cells, on their density or substrate colonization rate. The developed nanocomposite has controlled mechanical properties, high antibacterial activity and high biocompatibility, which makes it an attractive candidate for building and food package material manufacture and agriculture.

Keywords: poly(lactic)-co-glycolic acid; aluminum oxide nanoparticles; antibacterial activity; biocompatibility; reactive oxygen species; agriculture

1. Introduction

Packaging plays an important role in the food industry. Packaging material must protect food against any microbial, physical, chemical and environmental hazards during storage and transportation [1]. Petroleum-based plastics are widely used as packaging materials due to their lightweight nature, good barrier and other mechanical properties. Production of petroleum-based material is characterized by high speed and low cost [2,3]. Today, the production of plastic increased dramatically in the world. For example, it increased from 359 to 368 million tons during the years 2018–2019. The predicted production of plastic is 1800 million tons per year by 2050 [4,5]. Plastic materials used in food packaging are not biodegradable and their lifespan is 1–15 years and more [6,7]. Furthermore, the

plastic packages in the environment break down to fragments 0.5–5000 μm in size, which are called micro-plastics [8]. Accumulation of microplastics in animal bodies and plants was shown [9,10]. Microplastics can potentially lead to a wide range of disorders. For example, ingestion of microplastic particles leads to intestinal dysbacteriosis, inflammation and disturbance of reproductive health in mice [11,12]. Therefore, accumulation of plastic and microplastic in soil and water is a global ecological problem and development of eco-friendly and biodegradable package materials is an important goal of modern science and global industry [13].

Poly(lactic)-co-glycolic acid (PLGA) is a biosafe and biodegradable material. PLGA decomposes forming two non-toxic compounds polyglycolic (PGA) and polylactic (PLA) acids [14]. PLGA may be considered as biodegradable alternative of petroleum-based plastic for the use in food package manufacturing [5,15,16]. Advantages of PLGA as package materials are low cost of synthesis, opportunity to regulate in wide range physical properties such as tensile strength, glass transition temperatures, barrier properties, degradation time, biocompatibility, biodegradability, thermal stability, etc. [17]. These properties can be modified by changing the conditions of synthesis and by changing the proportions of initial compounds [18,19]. Unfortunately, biosafe and biocompatible materials can be a favorable substrate for bacterial colonization [20,21]. In this case, these materials could become the source of infection [22,23]. The problem of associated bacterial infection is complicated with the development of bacterial resistance to pesticides and antibiotics [24]. The addition of nanoparticles (NPs) of metals and their oxides in the polymer material is a way to overcome bacterial resistance to pesticides and antibiotics [25–27]. The mechanisms of antibacterial activity are common for NPs from a wide range of metal oxides and include: generation of reactive oxygen species (ROS) [28,29], genotoxic activity [30], inactivation of bacterial enzymes [31,32], disruption of the integrity of the bacterial cell wall, etc. [33–36]. A combination of polymer matrix with NPs is called nanocomposites. They can be used in various fields: textile and clothing production, construction, sensors development and medicine [37].

The global market size of nanotechnology in 2002 was about USD 110.6 billion and is predicted to grow to US\$ 891.1 billion in the near future [38]. Consumer goods production requires high amounts of nanomaterials, especially in packaging [38]. The biosafe polymers with antibacterial properties may also be applied in modern agriculture and biomedicine. Currently, the amount of publications on “nanocomposites” is more than 44,900, which includes “nanocomposites” + “package” >1800, “nanocomposites” + “agriculture” >1300 and “nanocomposites” + “biomedicine” >400 (Figure 1).

This amount has been constantly growing during the last 10 years. NPs and nanocomposites can be used as fertilizers, nanopesticides, food preservatives and as part of package material in agriculture [38–40]. The application of PLGA in medicine is described for stent development [3,41,42], for tissue regeneration with composites that contain growth factors [14,43], for target drug delivery or gene therapy, etc. [44–47].

The storage extension of consumer goods (for example fresh vegetables, fruits and meat) requires package material with high biocompatibility and extra low toxicity. In this case, the main limitation for metal and metal oxide NPs application is their toxicity to eukaryotic cells [48–51]. Aluminum oxide (Al_2O_3) is a cheap and non-reactive material with low toxicity for humans, animals and plants [52]. Al_2O_3 NPs also exhibit antibacterial properties [52]. The antibacterial activity of polymer composites with the addition of Al_2O_3 NPs was observed for both Gram-negative bacteria (*Escherichia coli*, *Pseudomonas aeruginosa*, etc.) and Gram-positive bacteria (*Bacillus subtilis*, *Staphylococcus aureus*, etc.) [53–56]. Moreover, the antifungal properties of nanocomposites with Al_2O_3 NPs are described [57,58].

In the present study, a nanocomposite based on PLGA and Al_2O_3 NPs has been developed. The nanocomposite has necessary mechanical properties for package materials manufacture. Additionally, it showed antibacterial activity and it did not affect the development and growth of plant and animal cells.

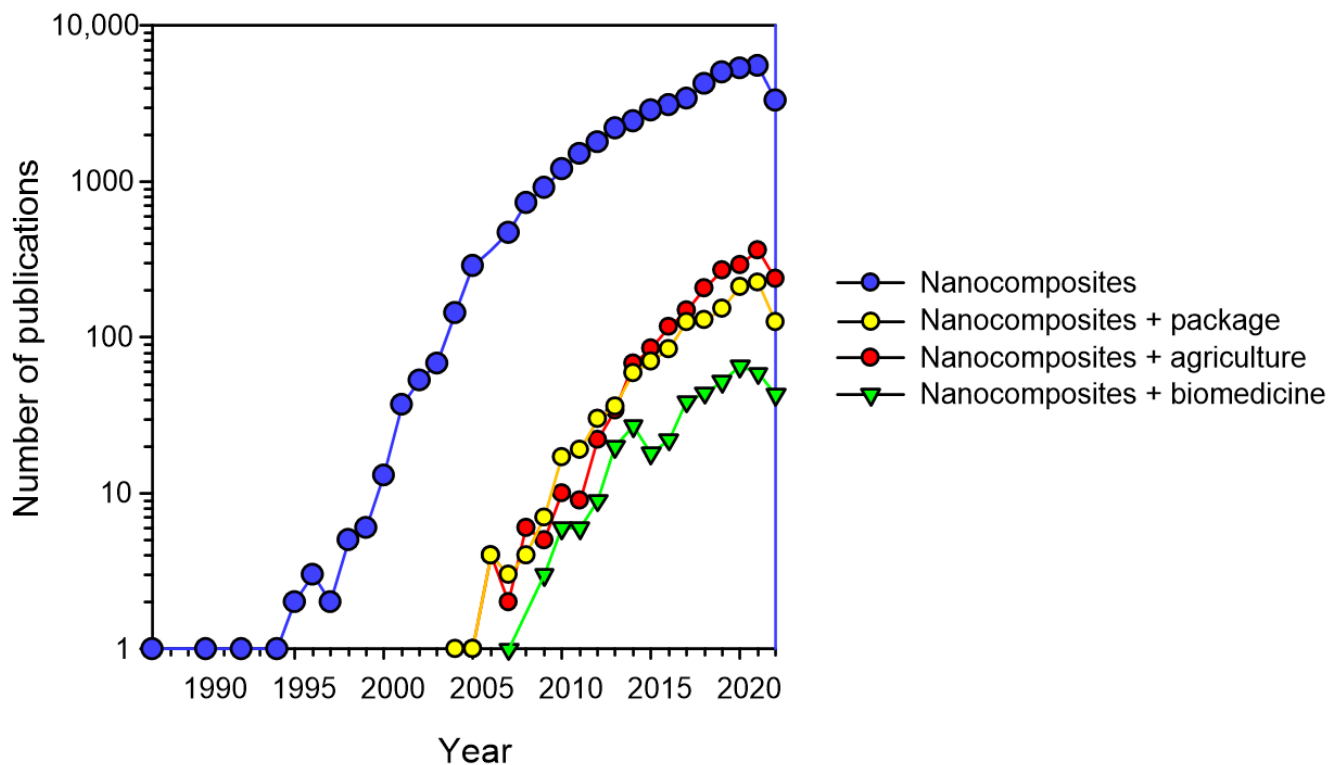


Figure 1. Number of publications devoted to nanocomposites (data 1 July 2022 <https://pubmed.ncbi.nlm.nih.gov/>).

2. Materials and Methods

2.1. Aluminum Oxide Nanoparticles Preparation and Characterization

Al_2O_3 NPs were obtained with laser ablation in water with ytterbium-doped fiber laser. Pulse parameters were $\lambda = 1064$ nm, $\tau = 4\text{--}200$ ns, energy 1 mJ, power ≤ 20 W. The aluminum Al (99.9%) was placed in 10 mL of deionized water so the thickness of the water layer over the metal target was ~ 1 mm. The Al was irradiated during 5 to 20 min with 20 kHz repetition frequency of laser pulses. The setup for the NPs synthesis with laser ablation is described in detail in [59].

The size and ζ -potential distribution of Al_2O_3 NPs were registered with dynamic light scattering method (DLS) on the Zetasizer Ultra Red Label (Malvern Panalytical, Malvern, UK). The technique is described in detail in [60]. The parameters such as: size, geometry and components of Al_2O_3 NPs were obtained with transmission electron microscopy (TEM) on the Libra 200 FE HR TEM microscope (Carl Zeiss, Oberkochen, Germany). The UV-visible spectra of NPs in water were recorded on the Cintra 4040 spectrophotometer (GBC Scientific Equipment, Melbourne, Australia). Modulation-interference microscope MIM-32 (Amphora Lab, Moscow, Russia) was used to evaluate the distribution of NPs inside the polymer matrix. The conditions of image recording were described in [61].

2.2. Composite Fabrication and Assay of Rheological Properties

The composite of PLGA and Al_2O_3 NPS was obtained with the low-temperature technology [62,63]. Briefly PLGA was diluted in ethanol, then NPs were added into the polymer and mixed afterwards. A control sample of PLGA was also diluted in ethanol. All samples were dried in a vacuum. The obtained nanopomposite was heated to 40°C and rolled up to film with thickness of 1000 μm . Subsequently, films were cut into pieces $20\text{ mm} \times 20\text{ mm}$ ($\sim 10\text{ cm}^2$) in size. Obtained pieces were immersed in 20 mL water.

2.3. Assay of Thermal Characteristics

Assay of thermal characteristics was performed with differential scanning calorimetry on the DSC 3 Excellence calorimeter (Mettler Toledo, Columbus, OH, USA). Thermograms were recorded in heating and cooling modes. Obtained thermograms were used to calculate thermal characteristics [64]. The glass transition temperature (T_g) and heat capacity change (ΔC_p) were calculated at different Al_2O_3 NPs concentrations.

2.4. Measurement of Hydrogen Peroxide Concentration

The hydrogen peroxide (H_2O_2) concentration was measured with chemiluminescence technique on the chemiluminometer Biotox-7A-USE (ANO Engineering Center—Ecology, Moscow, Russia). This method is based on oxidation of luminol with *p*-iodophenol catalyzed with peroxidase from horseradish [65]. The details of measurement and calibration can be found in [66]. Measurements were carried out in “counting solution” with samples which should be prepared immediately. “Counting solution” consists of Tris(hydroxymethyl)aminomethane hydrochloride (Tris-HCl) buffer (1 μM , pH 8.5) supplemented *p*-iodophenol (50 μM), luminol (50 μM) and horseradish peroxidase (10 nM). The H_2O_2 detection minimum is <1 nM [67].

2.5. Measurement of Hydroxyl-Radicals Concentration

The method is based on coumarin-3-carboxylic acid (CCA) hydrolysis to fluorophore 7-hydroxycoumarin-3-carboxylic acid (7-OH-CCA). Fluorescence intensity of 7-OH-CCA is proportional to hydroxyl-radicals (OH-radicals) concentration. Experimental samples and negative control were heated 2 h at 80 ± 0.1 °C in the presence of 0.5 mM CCA in PBS with pH 7.4. Fluorescence intensity was measured with spectrofluorometer JASCO 8300 (JASCO, Tokyo, Japan) at excitation wavelengths of 400 nm and emission wavelengths of 450 nm. A calibration curve was calculated beforehand using standard 7-OH-CCA solutions (Sigma Aldrich, St. Louis, MO, USA) [68].

2.6. Long-Lived Reactive Protein Species Detection

Chemiluminescence was used to evaluate the concentrations of long-lived reactive protein species (LRPS) in protein solutions after X-ray treatment [69]. X-rays induce free radicals recombination with subsequent emission of light quanta. The experiments were performed in a dark room at 25 °C. Measurements were carried out in plastic polypropylene vials for liquid scintillation counting (Beckman Coulter, Brea, CA, USA). The large volume (20 mL) was used in comparison with standard volume (0.1 mL) to improve (in ≤ 200 times) the sensitivity of the method [70]. All samples were irradiated by X-ray, then incubated 30 min after X-rays exposure, and chemiluminescence intensities were measured on the Biotox-7A-USE chemiluminometer (ANO Engineering Center—Ecology, Moscow, Russia). The untreated X-radiation proteins were used as a control. The detailed description of this method may be found in [71].

2.7. Measurement of 8-Oxoguanine Concentration

The concentration of 8-oxoguanine (8-oxo-Gua) in samples was measured with a non-competitive enzyme-linked immunosorbent assay (ELISA) with monoclonal antibodies against 8-oxo-Gua. Prior to this, the measurement samples of deoxyribonucleic acid (DNA) (350 $\mu\text{g}/\text{mL}$) were boiled in a water bath for 5 min and then cooled for 3–4 min in ice to induce DNA denaturation. Each sample (42 μL) was added into a well of a 98-well plate. Wells with samples were dried with incubation for 3 h at 80 °C to adsorb DNA on bottom surface of the plate. The blocking of nonspecific binding of antibodies to plate surface was done with incubation of samples with 300 μL of 1% skimmed milk in 0.15 M Tris-HCl buffer with pH 8.7, supplemented with 0.15 M sodium chloride (NaCl) overnight at room temperature. Wells were washed twice (300 $\mu\text{L}/\text{well}$) with 50 mM Tris-HCl buffer (pH 8.7) supplemented with 0.15 M NaCl and 0.1% Triton X-100. Further, 100 $\mu\text{L}/\text{well}$ of antibodies against 8-oxo-Gua were added in each well in an appropriate

dilution. Wells were washed twice after 20 min of incubation as described below. Further samples were incubated in a 80 μL /well solution of horseradish peroxidase-conjugated with secondary antibodies (1:1000 dilution) in a blocking buffer and afterwards were washed 3 times as described below. Subsequently, 100 μL of chromogenic substrate containing 18.2 mM 2,2'-azino-bis(3-ethylbenzthiazoline-6-sulfonic acid (ABTS) and hydrogen peroxide 2.6 mM in 75 mM citrate buffer with pH 4.2 was added in each well. After 15 min of incubation, a 50 μL /well of 1.5 mM sodium azide (NaN_3) in 0.1 M citrate buffer (pH 4.3) was added to stop the reaction [72]. The optical density of samples was evaluated at 405 nm on the photometer Titertek Multiscan (Labsystems, Vantaa, Finland). The method is described in detail in [73].

2.8. Assay of Bacteriostatic Activity

Gram-negative bacteria *Escherichia coli* were used as model microorganisms. All manipulations were carried out in sterile conditions. Initially, *E. coli* is cultured in a Petri dish with agar supplemented with Luria-Bertani medium (LB medium). A colony separated on agar was isolated and transferred in a glass culture tube with 5 mL LB medium. Then, the colony was resuspended in LB medium. The count of bacteria was evaluated with spectrophotometry on the UV5Nano Excellence spectrophotometer (Mettler Toledo, Columbus, OH, USA). The volume of analyzed medium with bacteria was 10 μL . Analyzed medium was not returned to the culture sample.

Nanocomposite films were made into a size of 10 mm \times 15 mm \times 1 mm. The films were sterilized by washing in ethyl alcohol three times within 30 min. Sterile films were placed on a round sterile hoop. Equal amount of *E. coli* in LB medium was added on the film samples, and then the top of the hoop was sealed with a glass slide. Samples were incubated at 37 $^\circ\text{C}$ for 24 h, and with 150 rpm in an ES-20 shaker-incubator (Biosan, Riga, Latvia). After incubation, the count of bacteria was estimated using a microscope (stained with crystal violet indicator) and drop spectrometer. Therefore, spectrophotometry and microscopy were simultaneously used; the concentration of microorganisms in the number of bacteria per unit area was obtained [74].

2.9. Measuring of Leaves Area

The experiments were carried out in a climatic chamber. Plants were grown in soil under standard conditions (illumination 16 h/day, temperature 22 $^\circ\text{C}$). The leaf area of tomatoes and cucumbers was measured with the GreenImage software developed by the research team [75]. The original digital images encoded in colors "Red-Green-Blue" (RGB images) of plant leaves were obtained in a vertical position with the same distance from the camera lens to the leaf. In order to select pixels corresponding to the image of leaves, the following procedure "IG = Ig - aIr - bIb" was used to select the green pixels, where Ig, Ir and Ib are the intensities of the red, green and blue color components of each pixel, respectively, IG is the resulting intensity of the selected green, and a, b are weight coefficients. Then, a threshold procedure was applied. The total number of pixels was multiplied to the area of one pixel in order to estimate the leaf area [76].

2.10. Assay of Biocompatibility with Mammalian Cells

Studies of biocompatibility were carried out on the human neuroblastoma cell line (SHSY5Y). The human neuroblastoma cell line SH-SY5Y (ATCC № CRL-2266, Manassas, VA, USA) was kindly provided by colleagues from the Department of Intracellular Signaling, Institute of Cell Biophysics, Russian Academy of Sciences, Pushchino, Russia. The SH-SY5Y is a canonical model for cytology and cytotoxicity assays. The SH-SY5Y cell line is a subclone of the neuroblastoma SK-N-SH cell line, isolated from the 4-year-old female patient. SH-SY5Y is widely used in the studies of cells proliferation, growth and differentiation [77]. The SH-SY5Y cells are cultured in an atmosphere supplied with 5% carbon dioxide (CO_2) in medium-contained DMEM (Biolot, St. Petersburg, Russia) 10% fetal bovine serum (Gibco, Waltham, MA, USA), 2 mM L-glutamine and 30 $\mu\text{g}/\text{mL}$ gentamicin (both Sigma Aldrich,

St. Louis, MO, USA). SH-SY5Y cells (10^4 cells/cm²) in a 3 mL culture medium were seeded on samples in Petri dishes (1 sample/dish) described above and incubated for three days. Cell viability was studied with fluorescent microscopy. Cells were loaded with 2 µg/mL Hoechst 33342 and 2 µg/mL propidium iodide (Sigma Aldrich, St. Louis, MO, USA) for 10 min at 37 °C. Hoechst 33342 and propidium iodide stained all cells in the sample and the death cells, respectively. Loaded cells were washed with phosphate buffer and immediately analyzed on the Leica DMI6000 (Leica, Wetzlar, Germany) confocal microscope. At least 500 cells were analyzed in each sample [78].

A proliferation assay was carried out after 72 h days of incubation of cell samples. An number of cells in a state of mitosis (mitotic index) was used to estimate proliferation rate. Cells were loaded with Hoechst 33342 for 15 min in order to contrast nuclei. Samples were analyzed on the fluorescence microscope. The total number of cells in the mitosis stage was evaluated. The mitotic index was calculated as a proportion of mitotic cell amount to the amount of all analyzed cells taken as 100% [79].

2.11. Statistic

All data are presented as means \pm SE. Data from at least three independent experiments were used in each experimental condition. Significance of differences between samples means was evaluated with the two sample two-tailed *t*-test. SigmaPlot software (v. 11.2, SPSS Inc. (Chicago, IL, USA)) were used for data statistical processing.

3. Results

The results of the analysis of the physical characteristics of Al₂O₃ NPs are shown in Figure 1. The distribution of Al₂O₃ NPs by the hydrodynamic radius determined on the DLS is unimodal. The mean size of NPs is 92 ± 7 nm (Figure 2a). According to transmission electron microscopy (TEM) data, the average NP size is ~ 80 nm (Figure 2b). The ζ -potential of Al₂O₃ NPs in water ranges from +30 to +70 mV, with a maximum of about +50 mV (Figure 2c), which indicates a high stability of the aqueous colloid of NPs. The UV-visible spectrum of NPs has a characteristic appearance for Al₂O₃ (Figure 2d). According to the data with energy dispersive X-ray spectrometry, aluminum and oxygen atoms are present in the NPs, in the ratio O/Al = 1.3 (Figure 3c), which may indicate the presence of Al₂O₃ and partially unoxidized Al in the NPs.

According to the results of atomic force microscopy (AFM), the nanocomposite has a smooth surface without defects and roughness (Figure 4a). Unfortunately, the AFM method does not allow for the evaluation of the distribution of NPs inside the polymer matrix. The optical properties (in particular the refractive index) of PLGA and Al₂O₃ significantly differ, so the distribution of Al₂O₃ NPs in the polymer thickness can be established with modulation interference microscopy (MIM) (Figure 5).

The refractive index of PLGA at 405 nm is ~ 1.47 . The refractive index of Al₂O₃ at 405 nm is ~ 1.79 . The difference between the values of the refractive indexes is more than 0.3, which makes it possible to identify NPs in the polymer matrix. It was found that PLGA without dopant does not contain pronounced internal structures. On the contrary, when Al₂O₃ NPs were added to the polymer matrix, domains with different phase shifts of the transmitted laser radiation were found in the composite. These domains were found at all studied concentrations of NPs 0.001–0.1% (Figure 5b–d).

At the same time, the intensity and size of domains increased with growth of Al₂O₃ NPs concentration and reached several micrometers. The obtained data indicate that Al₂O₃ NPs are not evenly distributed in the polymer. The concentration of NPs is quite high in some regions of the polymer matrix.

The results of thermal analysis are shown in Figure 6. For a polymer matrix without Al₂O₃ NPs, the values of heat capacity and glass transition temperature are ΔC_p and $T_g \sim 0.56$ J/(g \times K) and 319 K, respectively. The addition of Al₂O₃ NPs reduced the heat capacity of the composite compared to pure PLGA (Figure 6b). The effect is enhanced with an increase of the concentration of NPs. The effect of the dopant on T_g depends on the

concentration of Al_2O_3 NPs. At a concentration of NPs 0.001%, T_g decreased to ~ 317 K, at 0.01%, it did not change T_g and at 0.1%, T_g increased to ~ 322 K (Figure 6c).

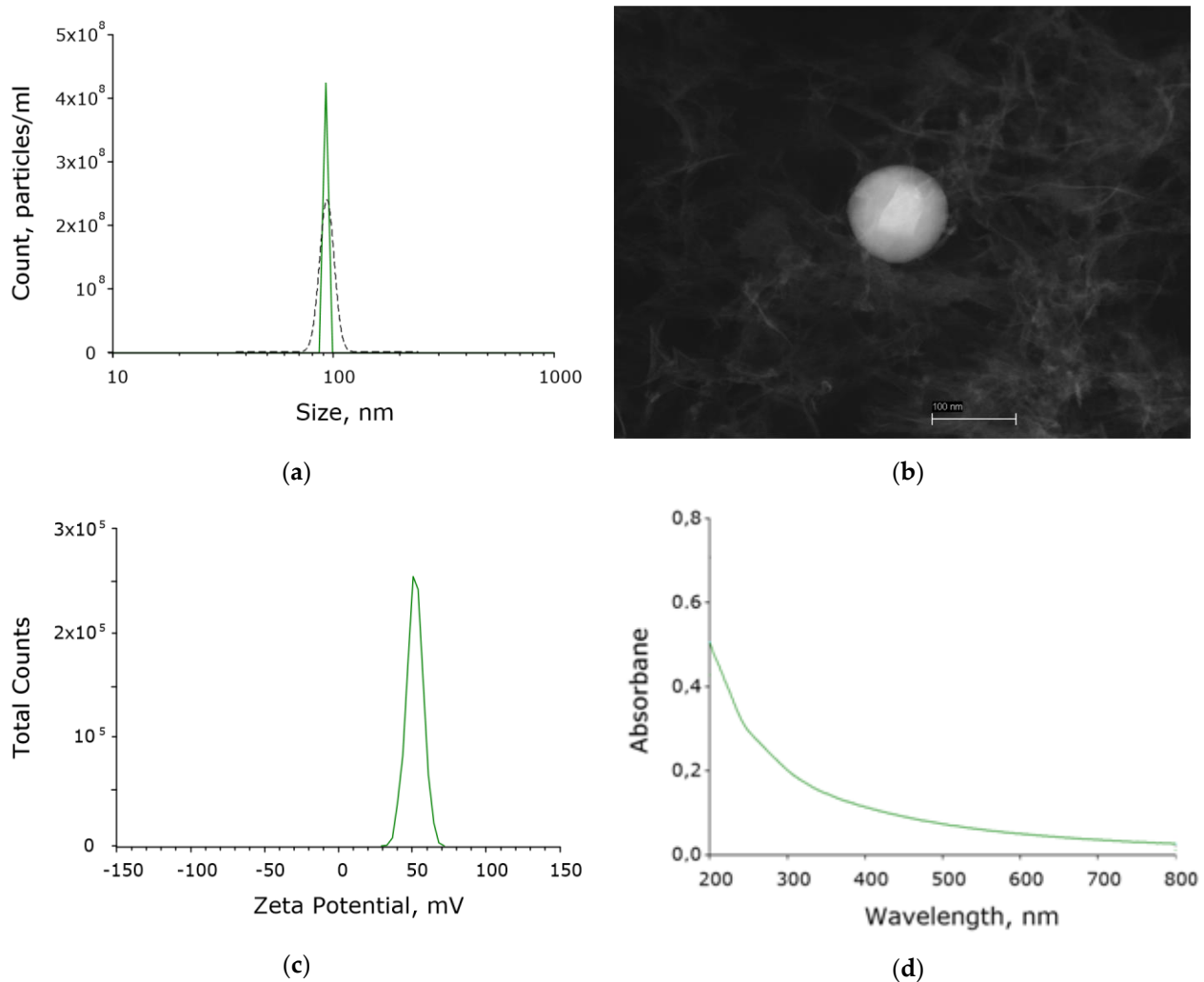
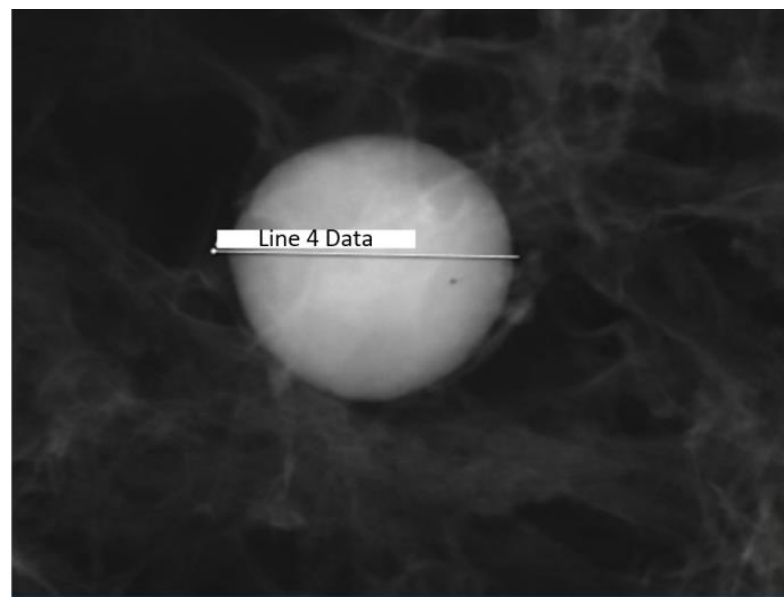


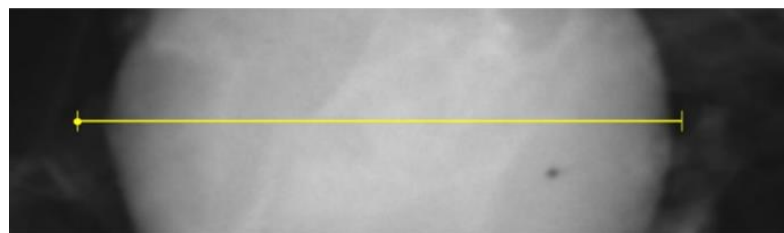
Figure 2. Physicochemical properties of Al_2O_3 NPs: (a) Concentration (DLS, green solid line) and size distribution (differential centrifugal sedimentation, black dashed line) of aluminium oxide NPs; (b) TEM image of aluminium oxide NP; (c) Zeta potential of aluminium oxide NPs; (d) Optical absorption of an aqueous colloidal solution of aluminium oxide NPs.

As mentioned earlier, generation of ROS is a more described mechanism of the antibacterial action of metal oxide NPs. The ability of the synthesized nanocomposite to generate key ROS: H_2O_2 (Figure 6a) and OH-radicals (Figure 6b)—was evaluated. Hydrogen peroxide is the most stable and long-lived ROS. OH-radicals are the most reactive ROS [80]. PLGA without dopant did not change the generation of both studied ROS. The addition of Al_2O_3 NPs impact on the generation of hydrogen peroxide (Figure 7a) and OH radicals (Figure 7b). It is essential that the effect depends on the Al_2O_3 NPs concentration.

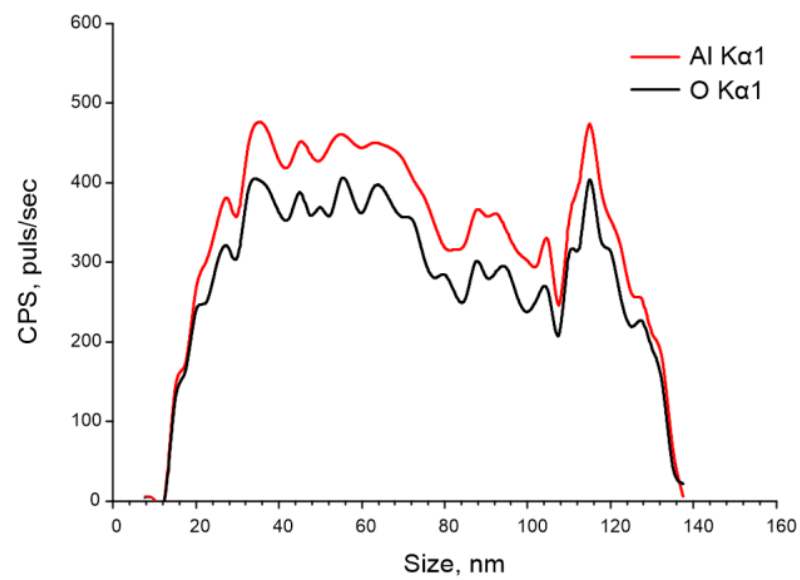
The highest level of ROS generation was found at a concentration of Al_2O_3 NPs of 0.1%—for both types of ROS. Presence of NPs at a concentration of 0.1% increased the generation of hydrogen peroxide and hydroxyl radical by ~ 3 and ~ 1.5 times, compared to PLGA without a dopant. ROS can damage biomolecules. The key markers of oxidative damage to biomacromolecules for DNA and proteins are 8-oxo-Gua and LRPS, respectively [81,82].



(a)



(b)



(c)

Figure 3. Elemental analysis of Al₂O₃ NPs: (a) TEM image of Al₂O₃ NP, analysis section is indicated with line 1; (b) Enlarged measurement site; (c) Nanoparticle profile by Al Kα1 and O Kα1.

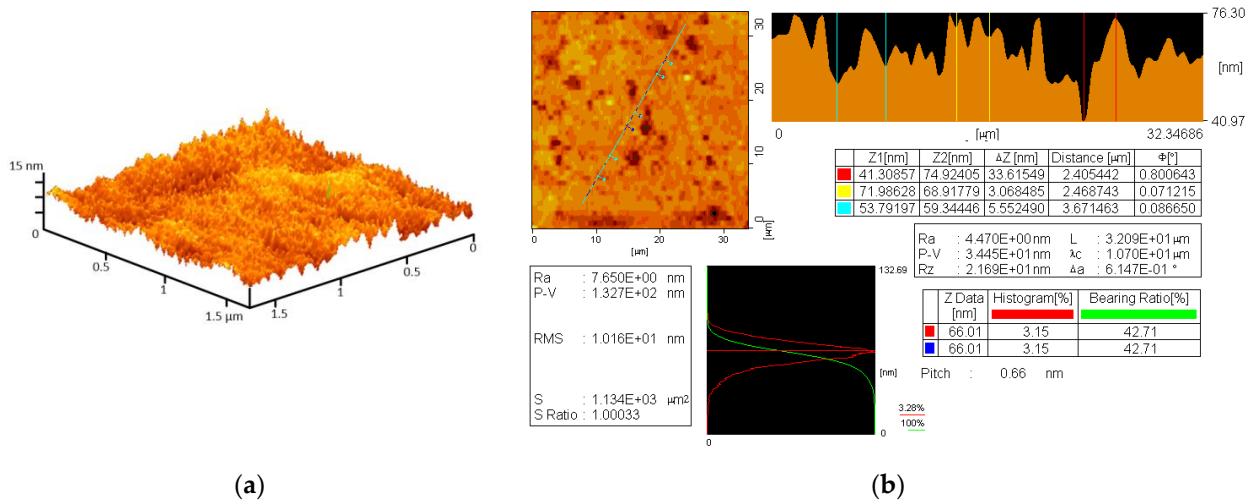


Figure 4. Reconstruction of nanocomposite surface with AFM: (a) 3D-reconstruction; (b) Example of results.

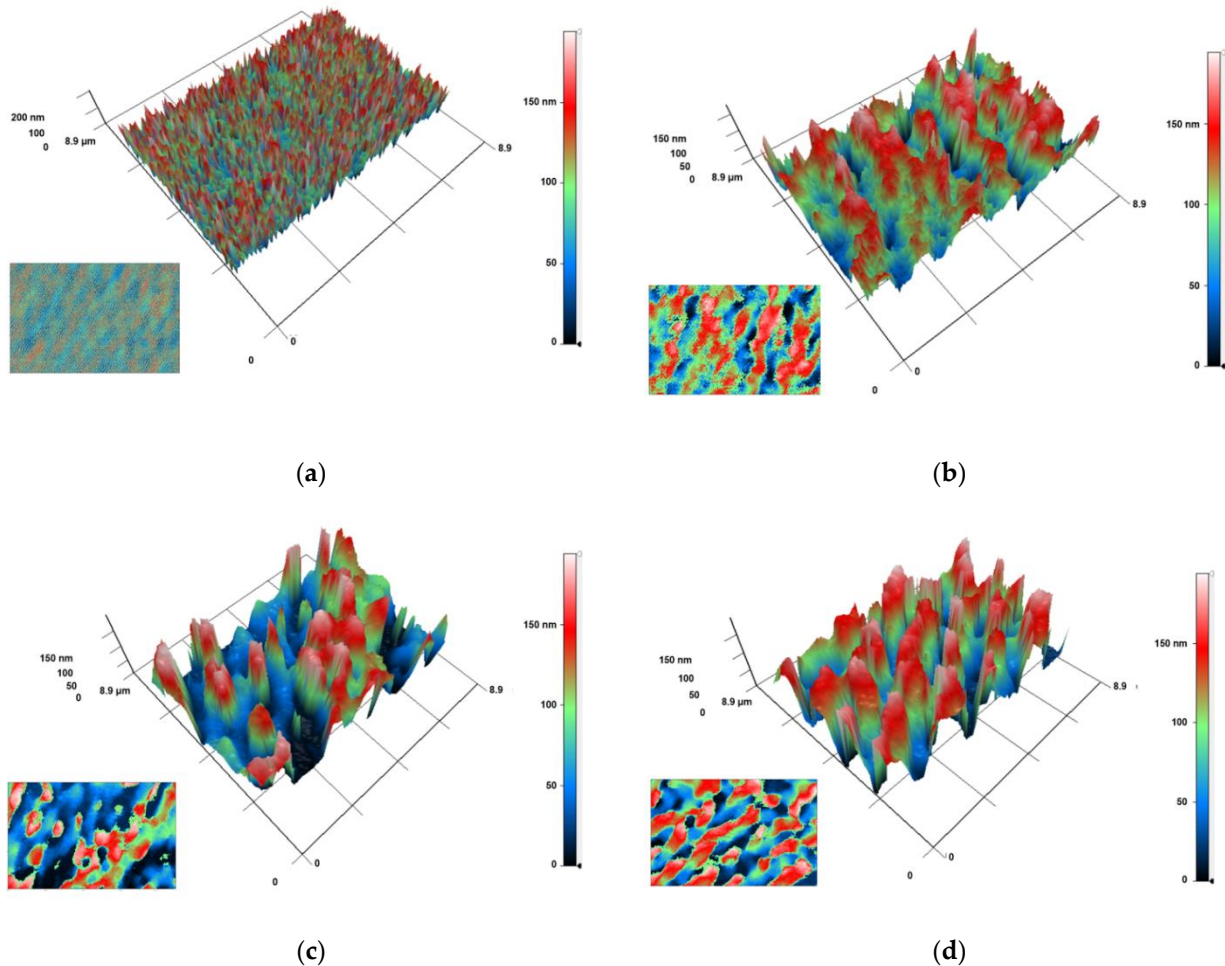


Figure 5. Images were obtained using a modulation interference microscope: (a) Polymer without NPs (b) and polymers with Al₂O₃ NPs at a concentration of 0.001%; (c) At a concentration of 0.01%; (d) At a concentration of 0.1%. Three-dimensional reconstructions of sample surfaces are presented. The X and Y axes show the actual size of the studied surfaces in micrometers. The Z-axis shows the surface relief as a phase change expressed in nm. Top view (surface elevation map) is shown in the lower left corner of each figure.

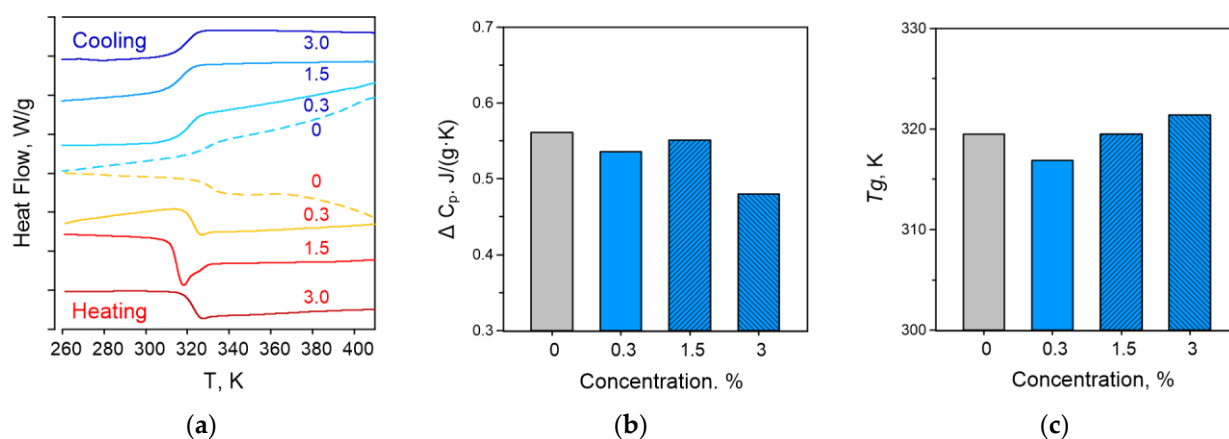


Figure 6. Results of thermal analysis and differential scanning calorimetry of nanocomposites: (a) Thermograms obtained in heating and cooling mode; (b) Glass transition temperatures of samples; (c) Change in the heat capacity.

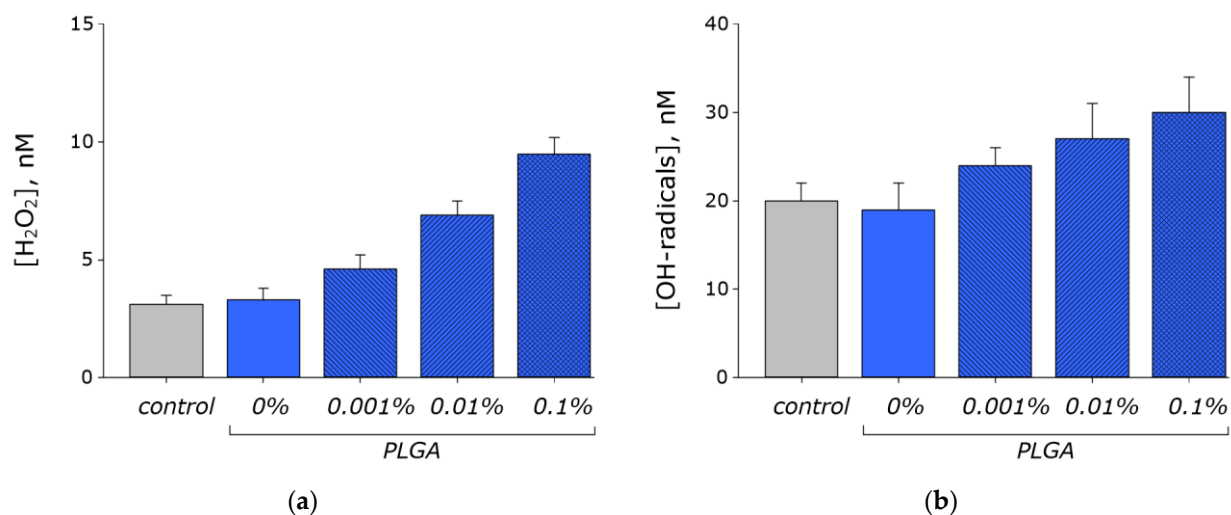


Figure 7. Effect of composite material containing PLGA and Al_2O_3 NPs on the generation of reactive oxygen species: (a) Generation of H_2O_2 (2 h, 40 °C); (b) Generation of OH-radicals (2 h, 80 °C); Data are presented as mean values and standard errors of mean.

The influence of the nanocomposite on the generation of 8-oxo-Gua and LRPS was studied (Figure 8). PLGA without dopant did not affect the generation of 8-oxo-Gua in DNA (Figure 8a). The addition of Al_2O_3 NPs increased the generation of 8-oxo-Gua in DNA (compared to PLGA without dopant) by 28, 64 and 92% at NP concentrations of 0.001, 0.01 and 0.1%, respectively. PLGA without dopant increased LRPS generation by 14% compared to control (Figure 8b). This effect was found only in the first hour after the experiment. After 3–5 h, no differences were found between the concentrations of LRPS in control and PLGA without dopant. The addition of Al_2O_3 NPs increased the generation of LRPS after 1 h (compared to PLGA without dopant) by 10, 18 and 32% at Al_2O_3 NP concentrations of 0.001, 0.01 and 0.1%, respectively. It should be noted that after 5 h in samples with 0.001, 0.01 and 0.1% Al_2O_3 NPs, the generation of LRPS was higher than in pure PLGA by 92, 98 and 144%, respectively. The half-life of LRPS did not depend on the concentration of Al_2O_3 NPs.

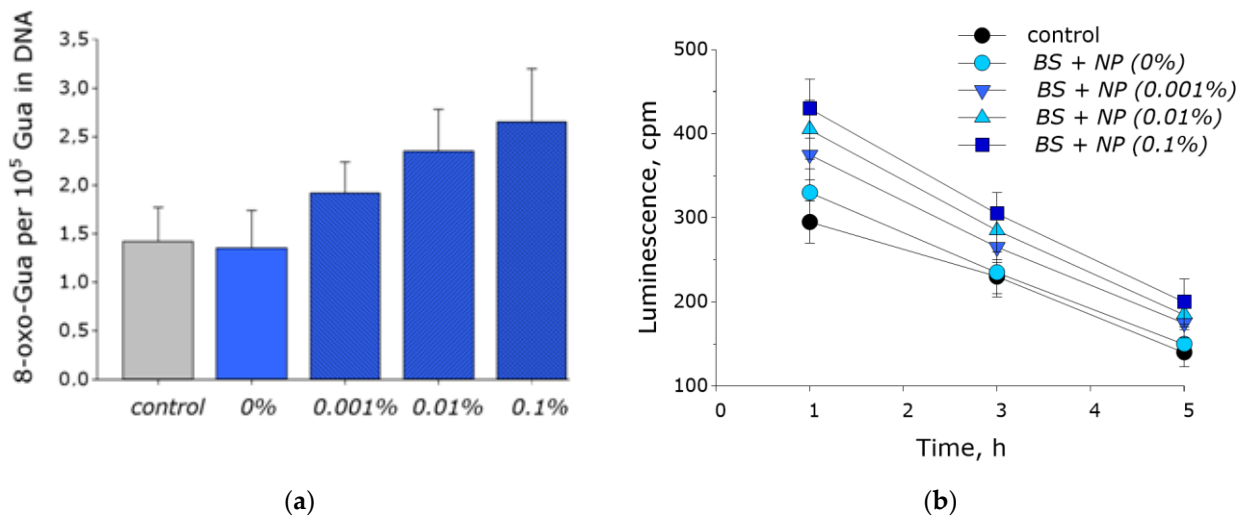


Figure 8. Effect of composite material containing PLGA and Al₂O₃ NPs on the biomacromolecules damage formation: (a) Generation of 8-oxo-Gua in DNA in vitro (2 h, 45 °C); (b) Generation and dynamics of decomposition of LRPS (2 h, 40 °C); Data are presented as mean values and standard errors of mean.

The effect of nanocomposite on the proliferation of *E. coli* bacteria was studied. PLGA without dopant and PLGA with 0.001% Al₂O₃ NPs did not change the growth rate of bacteria (Figure 9). An increase of Al₂O₃ NPs concentration to 0.01 and 0.1% reduced the growth of bacteria by 51 and 74%, respectively.

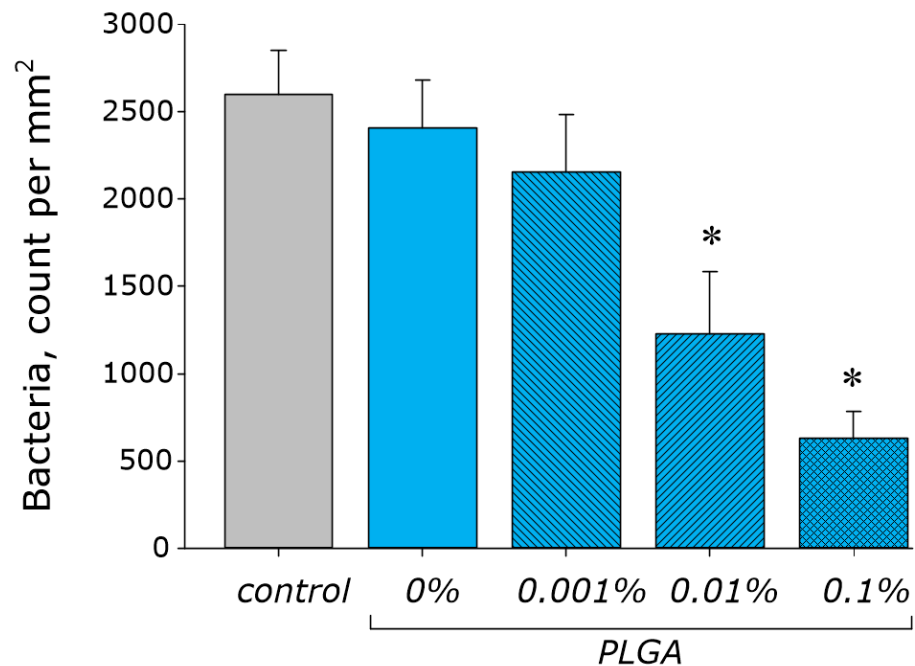
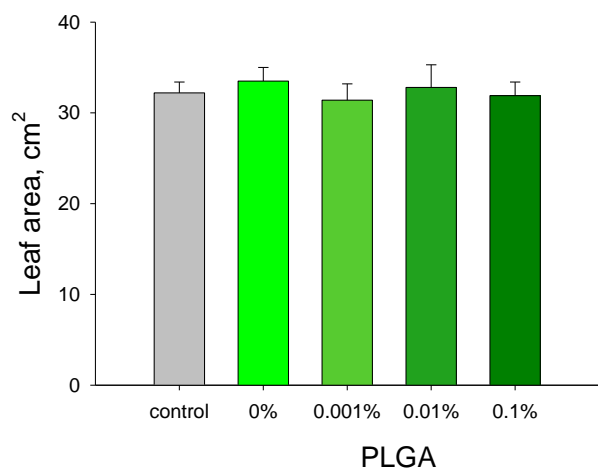


Figure 9. Influence of composite material based on PLGA and Al₂O₃ NPs on the growth and development of *E. coli*. *—significant difference at 5% level in comparison with the control ($p < 0.05$).

The effect of the nanocomposite based on PLGA and Al₂O₃ NPs on the growth rate of cucumbers (*Cucumis sativus*) and tomatoes (*Solanum lycopersicum*) has been studied. The growth rate was determined by the leaf area. Metal plates coated with a nanocomposite 0.5 cm wide were put into the soil to the entire depth of the vessel with soil at the rate of one plate per 10 cm² of soil area. It was shown that neither PLGA without dopant nor PLGA with Al₂O₃ NPs affected the growth rate of all studied plants (Figure 10).



(a)

(b)

Figure 10. Influence of a nanocomposite based on PLGA and Al₂O₃ NPs on the leaf size of plants: (a) Leaf size of *Solanum lycopersicum*. Data are presented as means and standard errors of the means; (b) Comparative photo of *Cucumis sativus* (plant in presence of nanocomposite is on the right).

To evaluate the biocompatibility of the developed nanocomposite with eukaryotic cells, the following parameters were measured: viability (the proportion of non-viable cells), mitotic index, cell density on the material, and area of the sample surface occupied with cells (Figure 10). Cell samples grown on culture plastic were used as controls. The growth of cell cultures on nanocomposite was compared with the growth on TiNbTaZr alloy in order to evaluate possibility of biomedical application of the technique. The percentage of non-viable cells on culture plastic was no more than 4% (Figure 11a). A slight trend towards an increase of the non-viable cells percentage was found for the growth on a nanocomposite. However, this trend did not reach statistical significance. The mitotic index of cells cultured on plastic was ~1.25% (Figure 11b). The mitotic index for the growth on the TiNbTaZr alloy was higher than for the control and it is ~1.76%. Cells cultured on all studied nanocomposites of PLGA and Al₂O₃ NPs had mitotic index values comparable with the control. The cell culture density for the control was (Figure 11c) ~1011 cells/mm². The cell culture density for the growth on the TiNbTaZr alloy was higher than for the control and it is ~1500 cells/mm². No differences in culture density from control were found for the growth of cells on PLGA without dopant and on PLGA with Al₂O₃ NPs of 0.001 and 0.01%. The density of cells on PLGA with 0.1% Al₂O₃ NPs was ~860 cells/mm² and it is lower than in the TiNbTaZr group but did not differ from the control values. The ability of a cell culture to populate the substrate surface was studied. Samples with complete confluence were not observed. At least 25% of the surface area was free from cells in all samples (Figure 11d). The free surface areas on PLGA both with and without NPs at all studied concentrations did not differ from the control (plastic) and is ~30%. When cells were cultivated on the TiNbTaZr alloy, the free surface area was lower—25%. Based on the obtained data, it has been concluded that the nanocomposite of PLGA and Al₂O₃ NPs has a high biocompatibility with mammalian cells (for example, SH-SY5Y culture). The biocompatibility of the nanocomposite is comparable with the culture plastic and is slightly higher than for the TiNbTaZr medical alloy. The values of the mitotic index, culture density and occupied surface area during cultivation on the nanocomposite do not depend on the concentration of Al₂O₃ NPs. Most likely, these parameters are primarily determined by the properties of the polymer matrix.

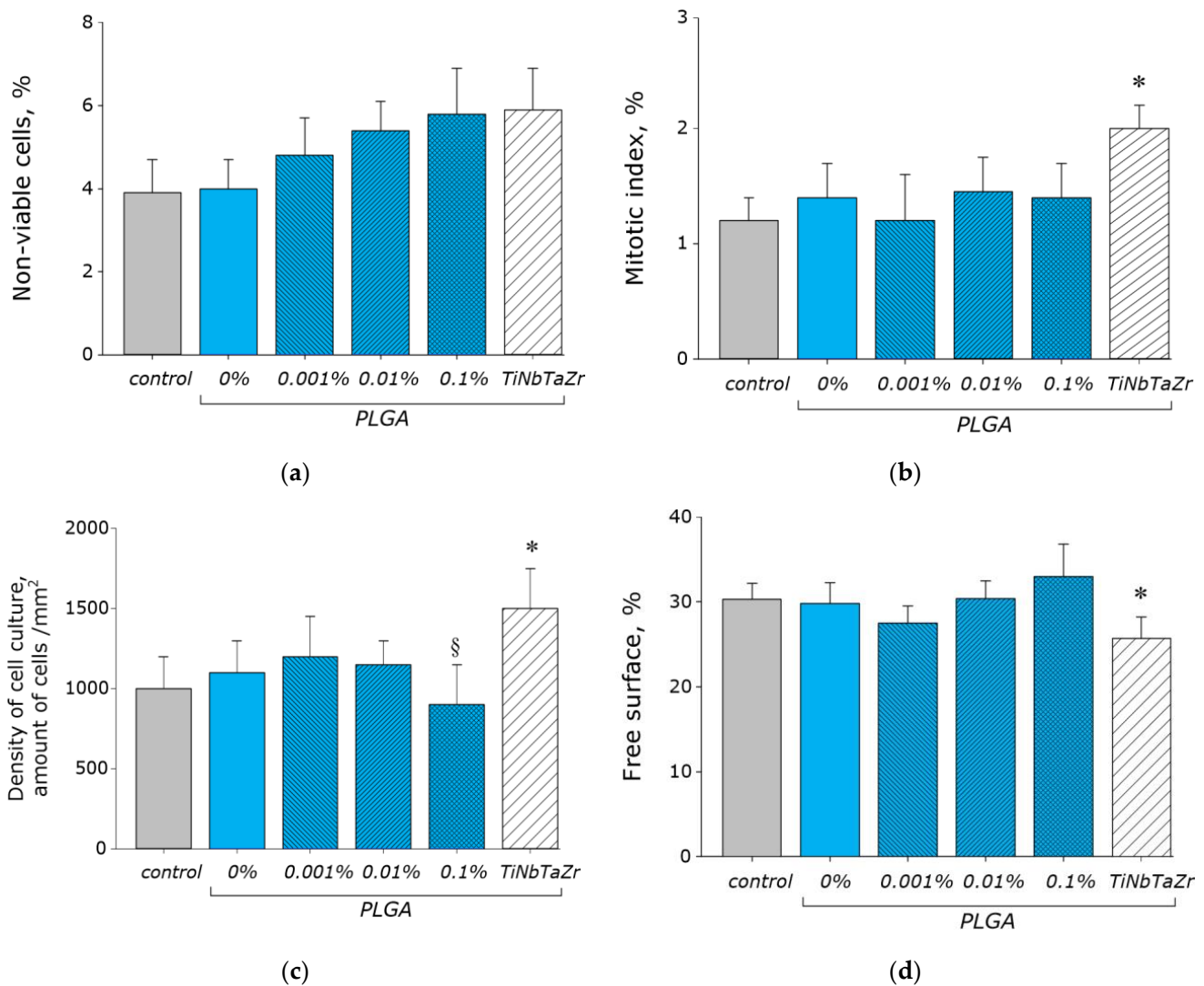


Figure 11. Effect of nanocomposite based on PLGA and Al₂O₃ NPs on the main characteristics of growth and development of mammalian cell culture: (a) Influence of nanocomposite on the viability of cell culture; (b) Influence of nanocomposite on the mitotic index; (c) Influence of nanocomposite on the cell culture density; (d) Influence of nanocomposite on the colonization rate of free surface by cells. *—indicates a significant difference in comparison with the control ($p < 0.05$). §—indicates a significant difference in comparison with the TiNbTaZr group ($p < 0.05$). Data are presented as mean values and standard errors of mean.

4. Discussion

Typically, nanocomposites based on polymers and NPs are used in packaging material [83], agriculture for photoconversion of solar radiation at high latitudes [84] and as a basis for covering material [85] and functional films [86]. At the same time, polymeric materials can be used in agriculture as structural materials for the manufacture of containers, overpasses and insulating materials. Most polymeric materials do not have antibacterial properties, although there is progress in this area. In this study, antibacterial properties were obtained by the use of manufactured nanoscale dopants based on Al₂O₃. Al₂O₃ NPs have been successfully synthesized with laser ablation in water. The size of the obtained NPs determined with DLS and TEM methods and it was 80–100 nm (Figure 2a,b). The average ζ-potential of Al₂O₃ NPs is +50 mV (Figure 2c). These values are higher than for commercially available NPs [87,88], which indicates a higher stability in aqueous colloidal solutions than with the NPs obtained in this research. The UV-visible spectrum of the NP colloid has the appearance characteristic of the UV spectra of Al₂O₃ NPs [89]. According to energy

dispersive X-ray spectrometry: aluminum and oxygen atoms are present in NPs in the ratio O/Al = 1.3 (Figure 3c). This ratio is lower than the expected value of 1.5—this fact, which indicates the possible presence in the NPs of not only Al₂O₃, but also metallic aluminum. It was shown that the surface of the nanocomposite is smooth (Figure 4). Using the MIM method, it was found that NPs are unevenly distributed inside the polymer matrix and form clusters (Figure 5). These data are consistent with previously obtained results for nanocomposites with PLGA [27].

The addition of Al₂O₃ NPs affected the glass transition temperature and heat capacity of the composite in a complex way, compared to PLGA without the dopant. The addition of 0.001% NP reduced both parameters, the addition of 0.01% NP did not change both parameters compared to pure PLGA and the addition of 0.1% Al₂O₃ NP increased the glass transition temperature (Figure 6b), but reduced the heat capacity (Figure 6c). According to the published research—changes in the heat capacity and glass transition temperature indicate a change in the internal viscosity of the polymer matrix [64]. The addition of Al₂O₃ NPs impacts the temperature properties of the nanocomposite, and this feature makes possible to control the internal viscosity of the polymer by changing the amount of added Al₂O₃ NPs at the stage of synthesis. The observed specifics of Al₂O₃ NPs distinguish them from silver oxide NPs obtained in the earlier studies [27]. Moreover, they make Al₂O₃ NPs a more attractive option for the manufacture of polymer composites with desired physical properties.

During the research of antibacterial properties of the developed nanocomposite, it has been found that PLGA without dopant did not affect the growth of *E. coli*. The addition of Al₂O₃ NPs at a concentration of 0.01 and 0.1% significantly inhibited bacterial growth (up to 51 and 74%, respectively, Figure 9). Thus, the minimum inhibitory concentration (MIC) of Al₂O₃ NPs in the nanocomposite corresponds to 10 µg/mL, which is comparable or significantly lower than in most studies [53,56–58,90–92]. A comparative analysis of the antimicrobial activities of nanocomposites based on Al₂O₃ NPs was performed on the grounds of the published studies (Table 1). It should be noted that the antimicrobial activity of nanocomposites of Al₂O₃ NPs depends on the type of polymer matrix and/or used coating. For example, chitosan- or polyaniline-coated Al₂O₃ NPs demonstrated less of an antibacterial (generally, bacteriostatic) effect in comparison to PLGA or borosilaxane-coated NP [53–55,59,62,93–96]. This fact can be explained with the intrinsic weak bacteriostatic and antibiofilm activity of PLGA [97]. PLGA/Al₂O₃ NPs composite had less antimicrobial activity (MIC 10 µg/mL) in comparison to PLGA-contained composites with ZnO, Fe₂O₃ or Ag₂O NPs (MIC 1 µg/mL) [62,93,94]. However, nanocomposites of PLGA/Fe₂O₃ NPs or PLGA/ZnO NPs decreased the viability of eukaryotic cells in a concentration of 100 µg/mL [62,94]. Nanocomposites of PLGA/Al₂O₃ NPs did not influence cell viability in all studied ranges of Al₂O₃ NPs concentrations. It could be explained by the lesser cytotoxicity of Al₂O₃ NPs for eukaryotic cells (excluding neurons) compared with NPs of others metals [24,36,98]. Therefore, the proportion between antibacterial activity and cytotoxicity of nanocomposites can be determined by choosing the oxide of metal in the NPs.

Table 1. Antimicrobial properties of Polymers/ Al₂O₃ NPs nanocomposites reported in other studies.

Nº	Composition	Size of NPs, nm	Microorganism Strains	Effect	MIC/MBC	Results	Reference
1	Commercially available Al ₂ O ₃ NPs coated with chitosan	<50	<i>Escherichia coli</i> ATCC2592, <i>Pseudomonas aeruginosa</i> ATCC 27853, <i>Staphylococcus epidermidis</i> ATCC 12228, <i>Staphylococcus aureus</i> ATCC 29213	bacteriostatic	5 mg/mL	Chitosan-coated Al ₂ O ₃ NPs realized bacteriostatic action due to binding with the active site of the target proteins for both Gram-positive and Gram-negative bacteria.	[53]
2	Commercially available Al ₂ O ₃ NPs coated with chitosan	80	<i>Staphylococcus aureus</i> ATCC 6538	bacteriostatic	25 µg/mL	Samples with chitosan had the highest level of antimicrobial activity (about 98%), which indicates high antibacterial activity of chitosan in the products.	[54]
3	γ-irradiated polyaniline (PANI)/Al ₂ O ₃ NPs composite	-	<i>Bacillus subtilis</i> , <i>Escherichia coli</i>	bacteriostatic	-	PANI–Al ₂ O ₃ NPs inhibited both Gram-positive and Gram-negative bacteria growth.	[55]
4	PANI/Al ₂ O ₃ NPs composite	14–19	<i>Escherichia coli</i> , <i>Staphylococcus aureus</i>	bacteriostatic	17 mg/mL	PANI–Al ₂ O ₃ NPs inhibited both Gram-positive and Gram-negative bacteria growth. The bacteriostatic was two times less than effect of amikacin.	[90]
5	Chitosan/Al ₂ O ₃ NPs	<10	<i>Aspergillus niger</i> NRRL A-326, <i>Candida albicans</i> ATCC 10231, <i>Pseudomonas aeruginosa</i> ATCC 27853, <i>Staphylococcus aureus</i> ATCC6538-P	bacteriostatic fungicidal	127 mg/mL	Chitosan/silica Al ₂ O ₃ NPs composite inhibited growth of <i>S. aureus</i> , <i>P. aeruginosa</i> and <i>C. albican</i> , but not <i>A. niger</i> .	[57]
6	Chitosan/P ₂ O ₅ :SiO ₂ -Al ₂ O ₃ NPs	100–800	<i>Aspergillus niger</i> , <i>Candida albicans</i> , <i>Pseudomonas aeruginosa</i> , <i>Staphylococcus aureus</i>	bacteriostatic fungicidal	654 mg/mL	The nanocomposite inhibited growth of all studied microorganisms in equal manner.	[58]
7	Borosilaxane/Al ₂ O ₃ NPs	45	<i>Escherichia coli</i>	bacteriostatic, bactericidal	10 µg/mL	Nanocomposite had antibacterial activity via generation of reactive species but did not change SH-SY5Y cell vitality.	[59]

Table 1. Cont.

Nº	Composition	Size of NPs, nm	Microorganism Strains	Effect	MIC/MBC	Results	Reference
8	Film of polylactic acid (PLA) contained Al ₂ O ₃ NPs or TiO ₂ -Al ₂ O ₃ NPs.	<10	<i>Escherichia coli</i> ATCC8739, <i>Pseudomonas aeruginosa</i> ATCC 10231	bacteriostatic	~15 mg/mL	The bacteriostatic effect of TiO ₂ -Al ₂ O ₃ nano-mixture against both bacteria was more effective than that Al ₂ O ₃ NPs.	[91]
9	Commercially available Al ₂ O ₃ or ZnO NPs added to cellulose acetate-chitosan membrane	<50	<i>Escherichia coli</i>	no	-	Authors did not observe bacteriostatic effect of Al ₂ O ₃ or ZnO NPs. Proposed case is the adsorption of NP on membrane.	[92]
10	Chitosan/ZnO-Al ₂ O ₃ NPs composite synthesized with sol-gel method.	<50	<i>Staphylococcus aureus</i>	bacteriostatic	20 mg/mL	Addition of ZnO NPs enhanced antibacterial activity of Chitosan-ZnO/Al ₂ O ₃ nanocomposites.	[95]
11	Commercially available Al ₂ O ₃ NPs mixed with cement building material	100	<i>Candida albicans</i> , <i>Escherichia coli</i> ATCC 8739, <i>Escherichia coli</i> MG1655, <i>Pseudomonas aeruginosa</i> , <i>Staphylococcus aureus</i>	bacteriostatic, bactericidal, fungicidal	125 µg/mL	Antimicrobial effect of Al ₂ O ₃ NPs depended on species. Maximum antimicrobial activity was observed versus <i>E. coli</i> (both strains) and <i>C. albicans</i>	[96]
12	PLGA/Ag ₂ O NPs	35	<i>Escherichia coli</i>	bacteriostatic, bactericidal	1 µg/mL	PLGA/Ag ₂ O NPs increased generation of ROS, damaged bacterial DNA and proteins, though didn't show cytotoxicity for eukaryotic cells.	[93]
13	PLGA/Fe ₂ O ₃ NPs	30	<i>Escherichia coli</i>	bacteriostatic, bactericidal	1 µg/mL	Nanocomposite increased generation of ROS, 8-oxo-Gua and LRPS inhibited bacterial growth. PLGA/Fe ₂ O ₃ NPs has low cytotoxicity at concentration 100 µg/mL. Nanocomposite did not interfere with plant growth.	[62]

Table 1. Cont.

Nº	Composition	Size of NPs, nm	Microorganism Strains	Effect	MIC/MBC	Results	Reference
14	PLGA/ZnO NPs	40–70	<i>Escherichia coli</i>	bacteriostatic, bactericidal	1 µg/mL	Nanocomposite inhibited bacterial growth but had no toxic effect on the development of eukaryotic cells.	[94]
15	PEG/PLGA NPs loaded with rutin and benzamide	260	<i>Pseudomonas aeruginosa</i> , <i>Staphylococcus aureus</i>	bacteriostatic, bactericidal	180 µg/mL	Drug-loaded PEG/PLGA NPs killed bacteria via cell wall disrupt. NPs demonstrated cytotoxicity for animal cell from concentration 40 µg/mL.	[97]
16	BSA/PLGA NPs loaded with sparfloxacin, tacrolimus and γ3-peptide	166–184	<i>Pseudomonas aeruginosa</i> , <i>Staphylococcus aureus</i>	bacteriostatic, bactericidal	1–4 µg/mL	Strong antibacterial activity. Bactericidal activity against Gram-positive bacteria was better.	[99]
17	PLGA-polyethyleneimine (PEI) NPs loaded with clindamycin	126–132	<i>Staphylococcus aureus</i> methicillin-resistant	bacteriostatic, bactericidal	300 µg/mL	Strong bactericidal activity. NPs did not change viability of L929 mouse fibroblast and improve wound healing in mice	[100]
18	PLGA/Al ₂ O ₃ NPs	80	<i>Escherichia coli</i>	bacteriostatic, bactericidal	10 µg/mL	PLGA/Al ₂ O ₃ NPs inhibited bacterial growth via ROS generation. Nanocomposite did not influence the growth of plants. PLGA/Al ₂ O ₃ NPs did not change human cell line viability and proliferation.	Present study

As mentioned earlier, the main mechanism of the antibacterial action of metal oxide NPs is the generation of ROS [101,102]. In order to test the implementation of this mechanism, the effect of the nanocomposite on ROS generation was evaluated (Figure 7). PLGA without a dopant did not cause the generation of hydrogen peroxide and hydroxyl radicals. This property distinguishes PLGA from a number of other polymers, in particular, ferrocene-containing polymers [103]. The addition of Al₂O₃ NPs increased the generation of both—H₂O₂ (Figure 7a) and OH-radical (Figure 7b). The greatest effect was observed at a NP concentration of 0.1%. At the same time, the rate of H₂O₂ generation increased by ~200%, and for the OH-radical by ~50%. It can be assumed that the antibacterial effect of the nanocomposite was realized exclusively due to Al₂O₃ NPs, which caused the generation of predominant H₂O₂. Since H₂O₂ is the most stable ROS [80], the presence of a prolonged antibacterial effect of the PLGA nanocomposite and Al₂O₃ NPs can be assumed. The key markers of oxidative damage to biomacromolecules DNA and proteins are 8-oxo-Gua and LRPS, respectively [81,82,104]. 8-oxo-Gua is able to induce GC-TA transversion during DNA replication, thereby exerting a powerful genotoxic effect [105,106]. LRPS is not only a marker of protein oxidative damage but is also capable of generating secondary radicals [22,82]. Pure PLGA did not change the generation of 8-oxo-Gua and LRPS, which favorably distinguishes PLGA from other materials [103]. The addition of Al₂O₃ NPs to PLGA increased the generation of 8-oxo-Gua in DNA compared to PLGA without dopant by 28, 64, and 92% at NP concentrations of 0.001, 0.01, and 0.1%, respectively (Figure 8a). The addition of Al₂O₃ NPs also increased the generation of LRPS compared to PLGA without dopant by 92, 98, and 144%, respectively (Figure 8b). The data obtained indicate that the antibacterial effect of Al₂O₃ NPs in the nanocomposite is realized due to oxidative damage to both DNA and proteins. At the same time, damage of the proteins is more pronounced.

It should be noted that, according to the MIM data, all NPs were compared with the polymer matrix (Figure 5). Consequently, the toxic effect of Al₂O₃ NPs is realized due to the release of aluminum cations Al³⁺ to the surrounding solution. The mechanisms of Al³⁺ toxicity are described in detail and include: activation of NADH oxidase and RPS generation, increase of the bacterial membrane permeability to other metals, phospholipid peroxidation and modification of bacterial proteins (enzymes and ionic channels) [107–110]. The electrostatic interaction of Al₂O₃ NP with bacterial cells, described in the [111], is excluded in this case, since all Al₂O₃ NP are incorporated into the polymer matrix (see above). However, the release of NPs is not excluded with a longer use of package material. The probability of NP release from the composite over time is, on the one hand, a guarantee of an additional antibacterial effect during long-term storage of food. On the other hand, it may be associated with the risk of the cytotoxicity of both the package and the product stored in it. The dynamics of the release of NPs from the nanocomposite is a task for further research.

No effect of the nanocomposite on the rate of plant growth and development was observed when cultivating plants in close proximity to rods coated with a nanocomposite based on PLGA and Al₂O₃ NPs 0.001–0.1% (Figure 10). The area of the leaves was comparable to the control. The size of the leaves does not always reflect the functional state of a plant. Functional parameters of the photosynthetic apparatus, for example, kinetics of chlorophyll a fluorescence, may be more informative [112]. Evaluation of the effect of nanocomposites on the physiological state of plants may be the goal of further research in this field.

When cultivating cells of the SH-SY5Y line on a nanocomposite based on PLGA and Al₂O₃ NPs (0.001–0.1%), all parameters for evaluating the state of cells (viability 4–6%, mitotic index 1.2–1.6%, culture density 950–1300 cells/mm² and the area of the surface occupied by cells, 27–32%) were comparable to the control (culture plastic). Therefore, the nanocomposite of PLGA and Al₂O₃ NPs has a high biocompatibility comparable to plastic for cell culture (Figure 11). Unfortunately, the absence of cytotoxicity *in vitro* does not guarantee high biocompatibility *in vivo*. In particular, aluminum, including Al₂O₃ NPs, has been shown to be highly neurotoxic [113,114]. In addition, the ability to accumulate in the lungs, liver, and kidneys was described for metal oxide NPs [115]. Experiments for *in vivo* evaluation of the biocompatibility are required for further development of

packaging materials or medical materials based on the PLGA/Al₂O₃ NPs nanocomposite. High biocompatibility (Figure 11) PLGA/Al₂O₃ NPs (more than TiNbTaZr) indicates the possibility of biomedical application of nanocomposite PLGA/Al₂O₃ NPs.

The search for new ways to improve antimicrobial activities of nanocomposites and/or also to add new activity is the aim of future studies. Conjugation of NPs, partially metal NPs, with antibiotics is one way to overcome bacterial antibiotic resistance and biofilm formation [97,99,100]. Mechanisms of antibacterial action of drug-conjugated NPs are the following: the damage of cell wall components, the protein denaturation, the increase of ROS production, the damage of DNA, etc. These properties were improved with controlled release of antibiotics [116]. Moreover, additional bioactive compounds can be loaded on NPs, for example, immunosuppressant or antioxidants [97,99].

The obtained results expand the knowledge about the mechanisms of toxicity of metal oxide NPs in combination with polymeric materials for bacteria, plants and mammalian cells. The results may find practical application for the development of eco-friendly materials, including food package, agriculture and biomedicine.

5. Conclusions

A new nanocomposite material based on PLGA and Al₂O₃ NPs has been synthesized. Al₂O₃ NPs were obtained with laser ablation in water. The synthesized NPs had unimodal size distributions of ~90 nm and a ζ potential of +50 mV. It has been found that the temperature properties (glass transition temperature and heat capacity) of the synthesized PLGA and Al₂O₃ NPs depend on the concentration of introduced NPs. In general, the physical properties of the nanocomposite can be controlled at the stage of the synthesis. The resulting nanocomposite significantly inhibited the growth and development of bacterial cells, though it did not affect the growth and development of plant and animal cells. The resulting nanocomposite can be a promising candidate for the manufacture of packaging materials, biomedicine and in agriculture.

Author Contributions: Conceptualization, A.V.S. (Alexander V. Simakin), V.I.B. and A.S.D.; methodology, R.M.S.; software, M.E.A.; validation, V.V.S. and A.V.S. (Alexey V. Shkirin); investigation, A.V.S. (Alexander V. Simakin), M.E.A., D.A.S., D.V.Y., D.N.C., O.V.U. and V.E.I.; resources, E.R. and A.S.; writing—original draft preparation, D.A.S.; writing—review and editing, A.V.S. (Alexander V. Simakin), A.S.D. and A.Y.I.; supervision, A.Y.I. All authors have read and agreed to the published version of the manuscript.

Funding: This research was funded by a grant from the Ministry of Science and Higher Education of the Russian Federation for large scientific projects in priority areas of scientific and technological development (subsidy identifier 075-15-2020-774).

Institutional Review Board Statement: Not applicable.

Informed Consent Statement: Not applicable.

Data Availability Statement: Not applicable.

Acknowledgments: The authors are grateful to the Shared Use Center of the GPI RAS.

Conflicts of Interest: The authors declare no conflict of interest.

References

1. Abdul Khalil, H.P.S.; Tye, Y.Y.; Leh, C.P.; Saurabh, C.K.; Ariffin, F.; Mohammad Fizree, H.; Mohamed, A.; Suriani, A.B. Cellulose Reinforced Biodegradable Polymer Composite Film for Packaging Applications. In *Bionanocomposites for Packaging Applications*; Springer: Berlin/Heidelberg, Germany, 2018; pp. 49–69. [[CrossRef](#)]
2. Wang, Y.; Zhang, Q.; Zhang, C.-I.; Li, P. Characterisation and cooperative antimicrobial properties of chitosan/nano-ZnO composite nanofibrous membranes. *Food Chem.* **2012**, *132*, 419–427. [[CrossRef](#)] [[PubMed](#)]
3. Kaplan, M.A.; Sergienko, K.V.; Kolmakova, A.A.; Konushkin, S.V.; Baikina, A.S.; Kolmakov, A.G.; Sevostyanov, M.A.; Kulikov, A.V.; Ivanov, V.E.; Belosludtsev, K.N.; et al. Development of a Biocompatible PLGA Polymers Capable to Release Thrombolytic Enzyme Prourokinase. *J. Biomater. Sci. Polym. Ed.* **2020**, *31*, 1405–1420. [[CrossRef](#)] [[PubMed](#)]

4. Taherimehr, M.; Yousefnipasha, H.; Tabatabaeeekolour, R.; Pesaranhajiabbas, E. Trends and challenges of biopolymer-based nanocomposites in food packaging. *Compr. Rev. Food Sci. Food Saf.* **2021**, *20*, 5321–5344. [[CrossRef](#)] [[PubMed](#)]
5. Jem, K.J.; Tan, B. The development and challenges of poly (lactic acid) and poly (glycolic acid). *Adv. Ind. Eng. Polym. Res.* **2020**, *3*, 60–70. [[CrossRef](#)]
6. Mangaraj, S.; Yadav, A.; Bal, L.M.; Dash, S.K.; Mahanti, N.K. Application of Biodegradable Polymers in Food Packaging Industry: A Comprehensive Review. *J. Packag. Technol. Res.* **2019**, *3*, 77–96. [[CrossRef](#)]
7. Pinheiro, I.F.; Ferreira, F.V.; Souza, D.H.S.; Gouveia, R.F.; Lona, L.M.F.; Morales, A.R.; Mei, L.H.I. Mechanical, rheological and degradation properties of PBAT nanocomposites reinforced by functionalized cellulose nanocrystals. *Eur. Polym. J.* **2017**, *97*, 356–365. [[CrossRef](#)]
8. Lim, X.Z. Microplastics are everywhere—But are they harmful? *Nature* **2022**, *593*, 22–25. [[CrossRef](#)] [[PubMed](#)]
9. Primpke, S.; Wirth, M.; Lorenz, C.; Gerdtts, G. Reference database design for the automated analysis of microplastic samples based on Fourier transform infrared (FTIR) spectroscopy. *Anal. Bioanal. Chem.* **2018**, *410*, 5131–5141. [[CrossRef](#)]
10. Jin, H.; Ma, T.; Sha, X.; Liu, Z.; Zhou, Y.; Meng, X.; Chen, Y.; Han, X.; Ding, J. Polystyrene microplastics induced male reproductive toxicity in mice. *J. Hazard. Mater.* **2021**, *401*, 123430. [[CrossRef](#)] [[PubMed](#)]
11. Li, B.; Ding, Y.; Cheng, X.; Sheng, D.; Xu, Z.; Rong, Q.; Wu, Y.; Zhao, H.; Ji, X.; Zhang, Y. Polyethylene microplastics affect the distribution of gut microbiota and inflammation development in mice. *Chemosphere* **2020**, *244*, 125492. [[CrossRef](#)] [[PubMed](#)]
12. Park, E.J.; Han, J.S.; Park, E.J.; Seong, E.; Lee, G.H.; Kim, D.W.; Son, H.Y.; Han, H.Y.; Lee, B.S. Repeated-oral dose toxicity of polyethylene microplastics and the possible implications on reproduction and development of the next generation. *Toxicol. Lett.* **2020**, *324*, 75–85. [[CrossRef](#)] [[PubMed](#)]
13. Sahoo, S.; Mohanty, S.; Nayak, S.K. Biobased polyurethane adhesive over petroleum based adhesive: Use of renewable resource. *J. Macromol. Sci. Part A* **2018**, *55*, 36–48. [[CrossRef](#)]
14. Eslami, H.; Azimi Lisar, H.; Jafarzadeh Kashi, T.S.; Tahriri, M.; Ansari, M.; Rafiei, T.; Bastami, F.; Shahin-Shamsabadi, A.; Mashhadi Abbas, F.; Tayebi, L. Poly(lactic-co-glycolic acid)(PLGA)/TiO₂ nanotube bioactive composite as a novel scaffold for bone tissue engineering: In vitro and in vivo studies. *Biol. J. Int. Assoc. Biol. Stand.* **2018**, *53*, 51–62. [[CrossRef](#)] [[PubMed](#)]
15. Jamshidian, M.; Tehrany, E.A.; Imran, M.; Jacquot, M.; Desobry, S. Poly-Lactic Acid: Production, Applications, Nanocomposites, and Release Studies. *Compr. Rev. Food Sci. Food Saf.* **2010**, *9*, 552–571. [[CrossRef](#)]
16. Biswal, A.K.; Thodikayil, A.T.; Saha, S. pH-Sensitive Acetalated Dextran/PLGA-Based Double-Layered Microparticles and Their Application in Food Preservation. *ACS Appl. Bio Mater.* **2021**, *4*, 2429–2441. [[CrossRef](#)]
17. Murcia Valderrama, M.A.; Van Putten, R.J.; Gruter, G.M. PLGA Barrier Materials from CO₂. The influence of Lactide Comonomer on Glycolic Acid Polyesters. *ACS Appl. Polym. Mater.* **2020**, *2*, 2706–2718. [[CrossRef](#)] [[PubMed](#)]
18. Haider, A.; Gupta, K.C.; Kang, I.K. PLGA/nHA hybrid nanofiber scaffold as a nanocargo carrier of insulin for accelerating bone tissue regeneration. *Nanoscale Res. Lett.* **2014**, *9*, 314. [[CrossRef](#)] [[PubMed](#)]
19. Haider, A.; Kwak, S.; Gupta, K.C.; Kang, I.-K. Antibacterial Activity and Cytocompatibility of PLGA/CuO Hybrid Nanofiber Scaffolds Prepared by Electrospinning. *J. Nanomater.* **2015**, *2015*, 832762. [[CrossRef](#)]
20. Davis, N.; Curry, A.; Gambhir, A.; Panigrahi, H.; Walker, C.; Wilkins, E.; Worsley, M.; Kay, P. Intraoperative bacterial contamination in operations for joint replacement. *J. Bone Jt. Surg. Br. Vol.* **1999**, *81*, 886–889. [[CrossRef](#)]
21. Nehra, P.; Chauhan, R.; Garg, N.; Verma, K. Antibacterial and antifungal activity of chitosan coated iron oxide nanoparticles. *Br. J. Biomed. Sci.* **2018**, *75*, 13–18. [[CrossRef](#)] [[PubMed](#)]
22. Thukkaram, M.; Sitaram, S.; Subbiahdoss, G. Antibacterial efficacy of iron-oxide nanoparticles against biofilms on different biomaterial surfaces. *Int. J. Biomater.* **2014**, *2014*, 716080. [[CrossRef](#)] [[PubMed](#)]
23. Hughes, S.; Anderson, F. *Infection in the Operating Room*; The British Editorial Society of Bone and Joint Surgery: London, UK, 1999.
24. Gudkov, S.V.; Burmistrov, D.E.; Serov, D.A.; Rebezov, M.B.; Semenova, A.A.; Lisitsyn, A.B. A Mini Review of Antibacterial properties of ZnO nanoparticles. *Front. Phys.* **2021**, *9*, 641481. [[CrossRef](#)]
25. Parmar, A.; Kaur, G.; Kapil, S.; Sharma, V.; Sachar, S.; Sandhir, R.; Sharma, S. Green chemistry mediated synthesis of PLGA-Silver nanocomposites for antibacterial synergy: Introspection of formulation parameters on structural and bactericidal aspects. *React. Funct. Polym.* **2019**, *141*, 68–81. [[CrossRef](#)]
26. Scavone, M.; Armentano, I.; Fortunati, E.; Cristofaro, F.; Mattioli, S.; Torre, L.; Kenny, J.M.; Imbriani, M.; Arciola, C.R.; Visai, L. Antimicrobial properties and cytocompatibility of PLGA/Ag nanocomposites. *Materials* **2016**, *9*, 37. [[CrossRef](#)]
27. Burmistrov, D.E.; Yanykin, D.V.; Pashkin, M.O.; Nagaev, E.V.; Efimov, A.D.; Kaziev, A.V.; Ageychenkov, D.G.; Gudkov, S.V. Additive Production of a Material Based on an Acrylic Polymer with a Nanoscale Layer of ZnO Nanorods Deposited Using a Direct Current Magnetron Discharge: Morphology, Photoconversion Properties, and Biosafety. *Materials* **2021**, *14*, 6586. [[CrossRef](#)]
28. Almatar, M.; Makky, E.A.; Var, I.; Koksai, F. The role of nanoparticles in the inhibition of multidrug-resistant bacteria and biofilms. *Curr. Drug Deliv.* **2018**, *15*, 470–484. [[CrossRef](#)]
29. Gold, K.; Slay, B.; Knackstedt, M.; Gaharwar, A.K. Antimicrobial Activity of Metal and Metal-Oxide Based Nanoparticles. *Adv. Ther.* **2018**, *1*, 1700033. [[CrossRef](#)]
30. Kohanski, M.A.; Depristo, M.A.; Collins, J.J. Sublethal antibiotic treatment leads to multidrug resistance via radical-induced mutagenesis. *Mol. Cell* **2010**, *37*, 311–320. [[CrossRef](#)]

31. Janani, B.; Al-Mohaimed, A.M.; Raju, L.L.; Al Farraj, D.A.; Thomas, A.M.; Khan, S.S. Synthesis and characterizations of hybrid PEG-Fe₃O₄ nanoparticles for the efficient adsorptive removal of dye and antibacterial, and antibiofilm applications. *J. Environ. Health Sci. Eng.* **2021**, *19*, 389–400. [[CrossRef](#)]
32. Yu, S.; Perálvarez-Marín, A.; Minelli, C.; Faraudo, J.; Roig, A.; Laromaine, A. Albumin-coated SPIONs: An experimental and theoretical evaluation of protein conformation, binding affinity and competition with serum proteins. *Nanoscale* **2016**, *8*, 14393–14405. [[CrossRef](#)]
33. Sousa, C.U.; Sequeira, D.; Kolen'ko, Y.V.; Pinto, I.S.M.; Petrovykh, D.Y. Analytical protocols for separation and electron microscopy of nanoparticles interacting with bacterial cells. *Anal. Chem.* **2015**, *87*, 4641–4648. [[CrossRef](#)] [[PubMed](#)]
34. Sirelkhatim, A.; Mahmud, S.; Seeni, A.; Kaus, N.H.M.; Ann, L.C.; Bakhori, S.K.M.; Hasan, H.; Mohamad, D. Review on Zinc Oxide Nanoparticles: Antibacterial Activity and Toxicity Mechanism. *Nano Micro Lett.* **2015**, *7*, 219–242. [[CrossRef](#)] [[PubMed](#)]
35. Gabrielyan, L.; Badalyan, H.; Gevorgyan, V.; Trchounian, A. Comparable antibacterial effects and action mechanisms of silver and iron oxide nanoparticles on *Escherichia coli* and *Salmonella typhimurium*. *Sci. Rep.* **2020**, *10*, 13145. [[CrossRef](#)]
36. Gudkov, S.V.; Burmistrov, D.E.; Smirnova, V.V.; Semenova, A.A.; Lisitsyn, A.B. A Mini Review of Antibacterial Properties of Al₂O₃ Nanoparticles. *Nanomaterials* **2022**, *12*, 2635. [[CrossRef](#)] [[PubMed](#)]
37. Gudkov, S.V.; Serov, D.A.; Astashev, M.E.; Semenova, A.A.; Lisitsyn, A.B. Ag₂O Nanoparticles as a Candidate for Antimicrobial Compounds of the New Generation. *Pharmaceuticals* **2022**, *15*, 968. [[CrossRef](#)]
38. Prasad, R.; Bhattacharyya, A.; Nguyen, Q.D. Nanotechnology in Sustainable Agriculture: Recent Developments, Challenges, and Perspectives. *Front. Microbiol.* **2017**, *8*, 1014. [[CrossRef](#)]
39. Martirosyan, A.; Schneider, Y.-J. Engineered Nanomaterials in Food: Implications for Food Safety and Consumer Health. *Int. J. Environ. Res. Public Health* **2014**, *11*, 5720–5750. [[CrossRef](#)]
40. Anu Bhushani, J.; Anandharamakrishnan, C. Electrospinning and electrospaying techniques: Potential food based applications. *Trends Food Sci. Technol.* **2014**, *38*, 21–33. [[CrossRef](#)]
41. Lin, L.-H.; Lee, H.-P.; Yeh, M.-L. Characterization of a sandwich PLGA-gallic acid-PLGA coating on Mg alloy ZK60 for biore-sorbable coronary artery stents. *Materials* **2020**, *13*, 5538. [[CrossRef](#)]
42. Sevostyanov, M.; Baikin, A.; Sergienko, K.; Shatova, L.; Kirsankin, A.; Baymler, I.; Shkirin, A.; Gudkov, S. Biodegradable stent coatings on the basis of PLGA polymers of different molecular mass, sustaining a steady release of the thrombolytic enzyme streptokinase. *React. Funct. Polym.* **2020**, *150*, 104550. [[CrossRef](#)]
43. Scheiner, K.C.; Maas-Bakker, R.F.; Van Steenberghe, M.J.; Schwendeman, S.P.; Hennink, W.E.; Kok, R.J. Post-loading of proan-giogenic growth factors in PLGA microspheres. *Eur. J. Pharm. Biopharm. Off. J. Arb. Fur Pharm. Verfahr. E.V* **2021**, *158*, 1–10. [[CrossRef](#)] [[PubMed](#)]
44. Sun, X.; Duan, Y.-R.; He, Q.; Lu, J.; Zhang, Z.-R. PELGE nanoparticles as new carriers for the delivery of plasmid DNA. *Chem. Pharm. Bull.* **2005**, *53*, 599–603. [[CrossRef](#)] [[PubMed](#)]
45. Kapoor, D.N.; Bhatia, A.; Kaur, R.; Sharma, R.; Kaur, G.; Dhawan, S. PLGA: A unique polymer for drug delivery. *Ther. Deliv.* **2015**, *6*, 41–58. [[CrossRef](#)] [[PubMed](#)]
46. Martins, C.; Sousa, F.; Araújo, F.; Sarmiento, B. Functionalizing PLGA and PLGA Derivatives for Drug Delivery and Tissue Regeneration Applications. *Adv. Healthc. Mater.* **2018**, *7*, 1701035. [[CrossRef](#)]
47. Klose, D.; Siepmann, F.; Elkharraz, K.; Siepmann, J. PLGA-based drug delivery systems: Importance of the type of drug and device geometry. *Int. J. Pharm.* **2008**, *354*, 95–103. [[CrossRef](#)] [[PubMed](#)]
48. Aazem, I.; Rathinam, P.; Pillai, S.; Honey, G.; Vengellur, A.; Bhat, S.G.; Sailaja, G. Active bayerite underpinned Ag₂O/Ag: An efficient antibacterial nanohybrid combating microbial contamination. *Metallomics* **2021**, *13*, mfab049. [[CrossRef](#)] [[PubMed](#)]
49. Beinert, H.; Holm, R.H.; Münck, E. Iron-sulfur clusters: Nature's modular, multipurpose structures. *Science* **1997**, *277*, 653–659. [[CrossRef](#)] [[PubMed](#)]
50. Calabrese, G.; Petralia, S.; Franco, D.; Nocito, G.; Fabbi, C.; Forte, L.; Guglielmino, S.; Squarzoni, S.; Traina, F.; Conoci, S. A new Ag-nanostructured hydroxyapatite porous scaffold: Antibacterial effect and cytotoxicity study. *Mater. Sci. Eng. C* **2021**, *118*, 111394. [[CrossRef](#)]
51. Franco, D.; Calabrese, G.; Petralia, S.; Neri, G.; Corsaro, C.; Forte, L.; Squarzoni, S.; Guglielmino, S.; Traina, F.; Fazio, E.; et al. Antimicrobial Effect and Cytotoxic Evaluation of Mg-Doped Hydroxyapatite Functionalized with Au-Nano Rods. *Molecules* **2021**, *26*, 1099. [[CrossRef](#)]
52. Liu, S.; Tian, J.; Zhang, W. Fabrication and application of nanoporous anodic aluminum oxide: A review. *Nanotechnology* **2021**, *32*, 222001. [[CrossRef](#)] [[PubMed](#)]
53. Abdel-Naby, A.S.; Nabil, S.; Aldulaijan, S.; Ababutain, I.M.; Alghamdi, A.I.; Almubayedh, S.; Khalil, K.D. Synthesis, Character-ization of Chitosan-Aluminum Oxide Nanocomposite for Green Synthesis of Annulated Imidazopyrazol Thione Derivatives. *Polymers* **2021**, *13*, 1160. [[CrossRef](#)]
54. Khajeh Mehrizi, M.; Mashroteh, H.; Nabizadeh Moghadam Noghabi, N. Effect of Chitosan, Aluminum Oxide and Silver Nanoparticles on Antibacterial, Deodorizing and Moisture Absorption Properties of Nonwoven Polyester Fabrics for Use in Medical Textiles. *Med. Lab. J.* **2016**, *10*, 46–52. [[CrossRef](#)]
55. Vyas, S.; Shukla, A.; Shivhare, S.; Upadhyay, N. Facile synthesis and characterization of polyaniline (PANI)—Aluminium oxide (Al₂O₃) nanocomposites by using chemical oxidative polymerization. *AIP Conf. Proc.* **2021**, *2369*, 020192. [[CrossRef](#)]
56. Manyasree, D.; Kiranmayi, P.; Ravi Kumar, R.V.S.S.N. Synthesis, characterization and antibacterial activity of aluminium oxide nanoparticles. *Int. J. Pharm. Pharm. Sci.* **2018**, *10*, 32–35. [[CrossRef](#)]

57. Nahrawy, A.M.E.; Abou Hammad, A.B.; Abdel-Aziz, M.S.; Wassel, A.R. Spectroscopic and Antimicrobial Activity of Hybrid Chitosan/Silica Membranes doped with Al₂O₃ Nanoparticles. *Silicon* **2019**, *11*, 1677–1685. [[CrossRef](#)]
58. El Nahrawy, A.M.; Mansour, A.M.; Abou Hammad, A.B.; Ibrahim, R.S.; Abouelnaga, A.M.; Abdel-Aziz, M.S. Optical, Functional Impact and Antimicrobial of Chitosan/Phosphosilicate/Al₂O₃ Nanosheets. *J. Inorg. Organomet. Polym. Mater.* **2020**, *30*, 3084–3094. [[CrossRef](#)]
59. Astashev, M.E.; Sarimov, R.M.; Serov, D.A.; Matveeva, T.A.; Simakin, A.V.; Ignatenko, D.N.; Burmistrov, D.E.; Smirnova, V.V.; Kurilov, A.D.; Mashchenko, V.I.; et al. Antibacterial behavior of organosilicon composite with nano aluminum oxide without influencing animal cells. *React. Funct. Polym.* **2022**, *170*, 105143. [[CrossRef](#)]
60. Sharapov, M.G.; Novoselov, V.I.; Penkov, N.V.; Fesenko, E.E.; Vedunova, M.V.; Bruskov, V.I.; Gudkov, S.V. Protective and adaptogenic role of peroxiredoxin 2 (Prx2) in neutralization of oxidative stress induced by ionizing radiation. *Free Radic. Biol. Med.* **2019**, *134*, 76–86. [[CrossRef](#)]
61. Sarimov, R.M.; Binhi, V.N.; Matveeva, T.A.; Penkov, N.V.; Gudkov, S.V. Unfolding and Aggregation of Lysozyme under the Combined Action of Dithiothreitol and Guanidine Hydrochloride: Optical Studies. *Int. J. Mol. Sci.* **2021**, *22*, 2710. [[CrossRef](#)] [[PubMed](#)]
62. Gudkov, S.V.; Burmistrov, D.E.; Lednev, V.N.; Simakin, A.V.; Uvarov, O.V.; Kucherov, R.N.; Ivashkin, P.I.; Dorokhov, A.S.; Izmailov, A.Y. Biosafety Construction Composite Based on Iron Oxide Nanoparticles and PLGA. *Inventions* **2022**, *7*, 61. [[CrossRef](#)]
63. Chausov, D.N.; Burmistrov, D.E.; Kurilov, A.D.; Bunkin, N.F.; Astashev, M.E.; Simakin, A.V.; Vedunova, M.V.; Gudkov, S.V. New Organosilicon Composite Based on Borosiloxane and Zinc Oxide Nanoparticles Inhibits Bacterial Growth, but Does Not Have a Toxic Effect on the Development of Animal Eukaryotic Cells. *Materials* **2021**, *14*, 6281. [[CrossRef](#)]
64. In Pyo Park, P.; Jonnalagadda, S. Predictors of glass transition in the biodegradable poly-lactide and poly-lactide-co-glycolide polymers. *J. Appl. Polym. Sci.* **2006**, *100*, 1983–1987. [[CrossRef](#)]
65. Gudkov, S.V.; Penkov, N.V.; Baimler, I.V.; Lyakhov, G.A.; Pustovoy, V.I.; Simakin, A.V.; Sarimov, R.M.; Scherbakov, I.A. Effect of mechanical shaking on the physicochemical properties of aqueous solutions. *Int. J. Mol. Sci.* **2020**, *21*, 8033. [[CrossRef](#)] [[PubMed](#)]
66. Barmina, E.; Gudkov, S.; Simakin, A.; Shafeev, G. Stable products of laser-induced breakdown of aqueous colloidal solutions of nanoparticles. *J. Laser Micro Nanoeng.* **2017**, *12*, 254–257. [[CrossRef](#)]
67. Baimler, I.V.; Lisitsyn, A.B.; Gudkov, S.V. Water decomposition occurring during laser breakdown of aqueous solutions containing individual gold, zirconium, molybdenum, iron or nickel nanoparticles. *Front. Phys.* **2020**, *8*, 600. [[CrossRef](#)]
68. Baimler, I.; Simakin, A.; Uvarov, O.; Volkov, M.Y.; Gudkov, S. Generation of hydroxyl radicals during laser breakdown of aqueous solutions in the presence of Fe and Cu nanoparticles of different sizes. *Phys. Wave Phenom.* **2020**, *28*, 107–110. [[CrossRef](#)]
69. Gudkov, S.V.; Garmash, S.A.; Shtarkman, I.N.; Chernikov, A.V.; Karp, O.E.; Bruskov, V.I. Long-lived protein radicals induced by X-ray irradiation are the source of reactive oxygen species in aqueous medium. *Doklady. Biochem. Biophys.* **2010**, *430*, 1–4. [[CrossRef](#)] [[PubMed](#)]
70. Sharapov, M.G.; Novoselov, V.I.; Fesenko, E.E.; Bruskov, V.I.; Gudkov, S.V. The role of peroxiredoxin 6 in neutralization of X-ray mediated oxidative stress: Effects on gene expression, preservation of radiosensitive tissues and postradiation survival of animals. *Free Radic. Res.* **2017**, *51*, 148–166. [[CrossRef](#)]
71. Sharapov, M.G.; Gudkov, S.V. Peroxiredoxin 1—Multifunctional antioxidant enzyme, protects from oxidative damages and increases the survival rate of mice exposed to total body irradiation. *Arch. Biochem. Biophys.* **2021**, *697*, 108671. [[CrossRef](#)]
72. Chernikov, A.V.; Gudkov, S.V.; Shtarkman, I.N.; Bruskov, V.I. Oxygen effect in heat-mediated damage to DNA. *Biofizika* **2007**, *52*, 244–251. [[CrossRef](#)] [[PubMed](#)]
73. Shtarkman, I.; Gudkov, S.; Chernikov, A.; Bruskov, V. Effect of amino acids on X-ray-induced hydrogen peroxide and hydroxyl radical formation in water and 8-oxoguanine in DNA. *Biochemistry* **2008**, *73*, 470–478. [[CrossRef](#)]
74. Barkhudarov, E.M.; Kossyi, I.A.; Anpilov, A.M.; Ivashkin, P.I.; Artem'ev, K.V.; Moryakov, I.V.; Misakyan, M.A.; Christofi, N.; Burmistrov, D.E.; Smirnova, V.V.; et al. New Nanostructured Carbon Coating Inhibits Bacterial Growth, but Does Not Influence on Animal Cells. *Nanomaterials* **2020**, *10*, 2130. [[CrossRef](#)]
75. Gudkov, S.V.; Simakin, A.V.; Bunkin, N.F.; Shafeev, G.A.; Astashev, M.E.; Glinushkin, A.P.; Grinberg, M.A.; Vodeneev, V.A. Development and application of photoconversion fluoropolymer films for greenhouses located at high or polar latitudes. *J. Photochem. Photobiol. B Biol.* **2020**, *213*, 112056. [[CrossRef](#)]
76. Burmistrov, D.E.; Yanykin, D.V.; Simakin, A.V.; Pashkin, M.O.; Ivanyuk, V.V.; Kuznetsov, S.V.; Ermakova, J.A.; Alexandrov, A.A.; Gudkov, S.V. Cultivation of Solanum lycopersicum under Glass Coated with Nanosized Upconversion Luminophore. *Appl. Sci.* **2021**, *11*, 10726. [[CrossRef](#)]
77. Sevostyanov, M.A.; Kolmakov, A.G.; Sergiyenko, K.V.; Kaplan, M.A.; Baikin, A.S.; Gudkov, S.V. Mechanical, physical–chemical and biological properties of the new Ti–30Nb–13Ta–5Zr alloy. *J. Mater. Sci.* **2020**, *55*, 14516–14529. [[CrossRef](#)]
78. Gudkov, S.V.; Simakin, A.V.; Sevostyanov, M.A.; Konushkin, S.V.; Losertová, M.; Ivannikov, A.Y.; Kolmakov, A.G.; Izmailov, A.Y. Manufacturing and study of mechanical properties, structure and compatibility with biological objects of plates and wire from new Ti–25Nb–13Ta–5Zr alloy. *Metals* **2020**, *10*, 1584. [[CrossRef](#)]
79. Konushkin, S.V.; Sergiyenko, K.V.; Nasakina, E.O.; Leontyev, V.G.; Kuznetsova, O.G.; Titov, D.D.; Tsareva, A.M.; Dormidontov, N.A.; Kirsankin, A.A.; Kannykin, S.V. Study of the physicochemical and biological properties of the new promising Ti–20Nb–13Ta–5Zr alloy for biomedical applications. *Mater. Chem. Phys.* **2020**, *255*, 123557. [[CrossRef](#)]

80. Gudkov, S.V.; Guryev, E.L.; Gapeyev, A.B.; Sharapov, M.G.; Bunkin, N.F.; Shkirin, A.V.; Zabelina, T.S.; Glinushkin, A.P.; Sevost'yanov, M.A.; Belosludtsev, K.N.; et al. Unmodified hydrated C(60) fullerene molecules exhibit antioxidant properties, prevent damage to DNA and proteins induced by reactive oxygen species and protect mice against injuries caused by radiation-induced oxidative stress. *Nanomed. Nanotechnol. Biol. Med.* **2019**, *15*, 37–46. [[CrossRef](#)]
81. Gudkov, S.V.; Shtarkman, I.N.; Chernikov, A.V.; Usacheva, A.M.; Bruskov, V.I. Guanosine and inosine (riboxin) eliminate the long-lived protein radicals induced X-ray radiation. *Doklady. Biochem. Biophys.* **2007**, *413*, 50–53. [[CrossRef](#)]
82. Bruskov, V.I.; Popova, N.R.; Ivanov, V.E.; Karp, O.E.; Chernikov, A.V.; Gudkov, S.V. Formation of long-lived reactive species of blood serum proteins by the action of heat. *Biochem. Biophys. Res. Commun.* **2014**, *443*, 957–961. [[CrossRef](#)]
83. Kozlova, E.S.; Nikiforova, T.E. Incorporation of silver nanoparticles into a cellulose matrix for preparing package materials for foodstuffs. *Russ. J. Appl. Chem.* **2015**, *88*, 638–646. [[CrossRef](#)]
84. Ivanyuk, V.V.; Shkirin, A.V.; Belosludtsev, K.N.; Dubinin, M.V.; Kozlov, V.A.; Bunkin, N.F.; Dorokhov, A.S.; Gudkov, S.V. Influence of Fluoropolymer Film Modified with Nanoscale Photoluminophor on Growth and Development of Plants. *Front. Phys.* **2020**, *8*, 616040. [[CrossRef](#)]
85. Khramov, R.; Kosobryukhov, A.; Kreslavski, V.; Balakirev, D.; Khudyakova, A.; Svidchenko, E.; Surin, N.; Ponomarenko, S.; Luponosov, Y. Luminescence of Agrotissues Based on Red-Light-Emitting Organic Luminophore and Polypropylene Spunbond Enhances the Growth and Photosynthesis of Vegetable Plants. *Front. Plant Sci.* **2022**, *13*, 827679. [[CrossRef](#)]
86. Chernov, A.S.; Reshetnikov, D.A.; Kovalitskaya Yu, A.; Manokhin, A.A.; Gudkov, S.V. Influence of wideband visible light with an padding red component on the functional state of mice embryos and embryonic stem cells. *J. Photochem. Photobiol. B Biol.* **2018**, *188*, 77–86. [[CrossRef](#)]
87. Mui, J.; Ngo, J.; Kim, B. Aggregation and Colloidal Stability of Commercially Available Al₂O₃ Nanoparticles in Aqueous Environments. *Nanomaterials* **2016**, *6*, 90. [[CrossRef](#)]
88. Choudhary, R.; Khurana, D.; Kumar, A.; Subudhi, S. Stability analysis of Al₂O₃/water nanofluids. *J. Exp. Nanosci.* **2017**, *12*, 140–151. [[CrossRef](#)]
89. Prashanth, P.A.; Raveendra, R.S.; Hari Krishna, R.; Ananda, S.; Bhagya, N.P.; Nagabhushana, B.M.; Lingaraju, K.; Raja Naika, H. Synthesis, characterizations, antibacterial and photoluminescence studies of solution combustion-derived α -Al₂O₃ nanoparticles. *J. Asian Ceram. Soc.* **2015**, *3*, 345–351. [[CrossRef](#)]
90. Ramakrishnan, S.; Rajakarthishan, S. Antimicrobial study on gamma-irradiated polyaniline–aluminum oxide (PANI–Al₂O₃) nanoparticles. *Int. Nano Lett.* **2020**, *10*, 97–110. [[CrossRef](#)]
91. Yakdouni, F.Z.; Hadj-Hamou, A.S. Effectiveness assessment of TiO₂-Al₂O₃ nano-mixture as a filler material for improvement of packaging performance of PLA nanocomposite films. *J. Polym. Eng.* **2020**, *40*, 848–858. [[CrossRef](#)]
92. Istirokhatun, T.; Yuni, U.; Andarani, P.; Susanto, H. Do ZnO and Al₂O₃ Nanoparticles Improve the Anti-Bacterial Properties of Cellulose Acetate-Chitosan Membrane? In *MATEC Web of Conferences*; EDP Sciences: Les Iles, France, 2018; Volume 156. [[CrossRef](#)]
93. Smirnova, V.V.; Chausov, D.N.; Serov, D.A.; Kozlov, V.A.; Ivashkin, P.I.; Pishchalnikov, R.Y.; Uvarov, O.V.; Vedunova, M.V.; Semenova, A.A.; Lisitsyn, A.B.; et al. A Novel Biodegradable Composite Polymer Material Based on PLGA and Silver Oxide Nanoparticles with Unique Physicochemical Properties and Biocompatibility with Mammalian Cells. *Materials* **2021**, *14*, 6915. [[CrossRef](#)]
94. Burmistrov, D.E.; Simakin, A.V.; Smirnova, V.V.; Uvarov, O.V.; Ivashkin, P.I.; Kucherov, R.N.; Ivanov, V.E.; Bruskov, V.I.; Sevostyanov, M.A.; Baikin, A.S.; et al. Bacteriostatic and Cytotoxic Properties of Composite Material Based on ZnO Nanoparticles in PLGA Obtained by Low Temperature Method. *Polymers* **2021**, *14*, 49. [[CrossRef](#)] [[PubMed](#)]
95. Maharani, D.K.; Hidayah, R.; Khasanah, L. Qualitative Study of Antibacterial Activity of Chitosan-ZnO/Al₂O₃ Nanocomposites. *Adv. Sci. Lett.* **2017**, *23*, 11948–11951. [[CrossRef](#)]
96. Sikora, P.; Augustyniak, A.; Cendrowski, K.; Nawrotek, P.; Mijowska, E. Antimicrobial Activity of Al₂O₃, CuO, Fe₃O₄, and ZnO Nanoparticles in Scope of Their Further Application in Cement-Based Building Materials. *Nanomaterials* **2018**, *8*, 212. [[CrossRef](#)]
97. Deepika, M.S.; Thangam, R.; Sundarraj, S.; Sheena, T.S.; Sivasubramanian, S.; Kulandaivel, J.; Thirumurugan, R. Co-delivery of Diverse Therapeutic Compounds Using PEG–PLGA Nanoparticle Cargo against Drug-Resistant Bacteria: An Improved Anti-biofilm Strategy. *ACS Appl. Bio Mater.* **2020**, *3*, 385–399. [[CrossRef](#)]
98. Gudkov, S.V.; Burmistrov, D.E.; Serov, D.A.; Rebezov, M.B.; Semenova, A.A.; Lisitsyn, A.B. Do Iron Oxide Nanoparticles Have Significant Antibacterial Properties? *Antibiotics* **2021**, *10*, 884. [[CrossRef](#)] [[PubMed](#)]
99. Yang, Y.; Ding, Y.; Fan, B.; Wang, Y.; Mao, Z.; Wang, W.; Wu, J. Inflammation-targeting polymeric nanoparticles deliver sparfloxacin and tacrolimus for combating acute lung sepsis. *J. Control. Release* **2020**, *321*, 463–474. [[CrossRef](#)] [[PubMed](#)]
100. Hasan, N.; Cao, J.; Lee, J.; Hlaing, S.P.; Oshi, M.A.; Naem, M.; Ki, M.-H.; Lee, B.L.; Jung, Y.; Yoo, J.-W. Bacteria-Targeted Clindamycin Loaded Polymeric Nanoparticles: Effect of Surface Charge on Nanoparticle Adhesion to MRSA, Antibacterial Activity, and Wound Healing. *Pharmaceutics* **2019**, *11*, 236. [[CrossRef](#)]
101. Fu, P.P.; Xia, Q.; Hwang, H.-M.; Ray, P.C.; Yu, H. Mechanisms of nanotoxicity: Generation of reactive oxygen species. *J. Food Drug Anal.* **2014**, *22*, 64–75. [[CrossRef](#)]
102. Valko, M.; Morris, H.; Cronin, M. Metals, toxicity and oxidative stress. *Curr. Med. Chem.* **2005**, *12*, 1161–1208. [[CrossRef](#)]
103. Na, Y.; Lee, J.S.; Woo, J.; Ahn, S.; Lee, E.; Choi, W.I.; Sung, D. Reactive oxygen species (ROS)-responsive ferrocene-polymer-based nanoparticles for controlled release of drugs. *J. Mater. Chem. B* **2020**, *8*, 1906–1913. [[CrossRef](#)]

104. Bruskov, V.I.; Karp, O.E.; Garmash, S.A.; Shtarkman, I.N.; Chernikov, A.V.; Gudkov, S.V. Prolongation of oxidative stress by long-lived reactive protein species induced by X-ray radiation and their genotoxic action. *Free Radic. Res.* **2012**, *46*, 1280–1290. [[CrossRef](#)] [[PubMed](#)]
105. Cohen, H.; Levy, R.; Gao, J.; Fishbein, I.; Kousaev, V.; Sosnowski, S.; Slomkowski, S.; Golomb, G. Sustained delivery and expression of DNA encapsulated in polymeric nanoparticles. *Gene Ther.* **2000**, *7*, 1896–1905. [[CrossRef](#)] [[PubMed](#)]
106. Karp, O.E.; Gudkov, S.V.; Garmash, S.A.; Shtarkman, I.N.; Chernikov, A.V.; Bruskov, V.I. Genotoxic effect of long-lived protein radicals in vivo generated by X-ray irradiation. *Doklady. Biochem. Biophys.* **2010**, *434*, 250–253. [[CrossRef](#)] [[PubMed](#)]
107. Xia, T.; Kovoichich, M.; Brant, J.; Hotze, M.; Sempf, J.; Oberley, T.; Sioutas, C.; Yeh, J.I.; Wiesner, M.R.; Nel, A.E. Comparison of the Abilities of Ambient and Manufactured Nanoparticles to Induce Cellular Toxicity According to an Oxidative Stress Paradigm. *Nano Lett.* **2006**, *6*, 1794–1807. [[CrossRef](#)] [[PubMed](#)]
108. Londono, S.C.; Hartnett, H.E.; Williams, L.B. Antibacterial Activity of Aluminum in Clay from the Colombian Amazon. *Environ. Sci. Technol.* **2017**, *51*, 2401–2408. [[CrossRef](#)]
109. Gutteridge, J.M.C.; Quinlan, G.J.; Clark, I.; Halliwell, B. Aluminium salts accelerate peroxidation of membrane lipids stimulated by iron salts. *Biochim. Biophys. Acta Lipids Lipid Metab.* **1985**, *835*, 441–447. [[CrossRef](#)]
110. Morrison, K.D.; Misra, R.; Williams, L.B. Unearthing the Antibacterial Mechanism of Medicinal Clay: A Geochemical Approach to Combating Antibiotic Resistance. *Sci. Rep.* **2016**, *6*, 19043. [[CrossRef](#)]
111. Slavin, Y.N.; Asnis, J.; Häfeli, U.O.; Bach, H. Metal nanoparticles: Understanding the mechanisms behind antibacterial activity. *J. Nanobiotechnol.* **2017**, *15*, 65. [[CrossRef](#)]
112. Yanykin, D.V.; Pashkin, M.O.; Simakin, A.V.; Burmistrov, D.E.; Pobedonostsev, R.V.; Vyatchinov, A.A.; Vedunova, M.V.; Kuznetsov, S.V.; Ermakova, J.A.; Alexandrov, A.A.; et al. Plant Photochemistry under Glass Coated with Upconversion Luminescent Film. *Appl. Sci.* **2022**, *12*, 7480. [[CrossRef](#)]
113. Mirshafa, A.; Nazari, M.; Jahani, D.; Shaki, F. Size-Dependent Neurotoxicity of Aluminum Oxide Particles: A Comparison Between Nano- and Micrometer Size on the Basis of Mitochondrial Oxidative Damage. *Biol. Trace Elem. Res.* **2018**, *183*, 261–269. [[CrossRef](#)]
114. Dey, M.; Singh, R.K. Neurotoxic effects of aluminium exposure as a potential risk factor for Alzheimer’s disease. *Pharmacol. Rep.* **2022**, *74*, 439–450. [[CrossRef](#)]
115. Hanini, A.; Schmitt, A.; Kacem, K.; Chau, F.; Ammar, S.; Gavard, J. Evaluation of iron oxide nanoparticle biocompatibility. *Int. J. Nanomed.* **2011**, *6*, 787.
116. Thambirajoo, M.; Maarof, M.; Lokanathan, Y.; Katas, H.; Ghazalli, N.F.; Tabata, Y.; Fauzi, M.B. Potential of Nanoparticles Integrated with Antibacterial Properties in Preventing Biofilm and Antibiotic Resistance. *Antibiotics* **2021**, *10*, 1338. [[CrossRef](#)] [[PubMed](#)]